Coherent sea level variation in and around the Sea of Okhotsk

Takuya Nakanowatari *, Kay I. Ohshima

Institute of Low Temperature Science, Hokkaido University, Sapporo, Japan

* Corresponding author address.

Institute of Low Temperature Science, Hokkaido University

Kita-19, Nishi-8, Sapporo, 060-0819 Japan

Tel.:+81-11-706-5497 ; fax:+81-11-706-5497 .

E-mail address: nakano@lowtem.hokudai.ac.jp (T. Nakanowatari).

ABSTRACT

We investigated the seasonal and interannual variations of the sea level in and around the Sea of Okhotsk and their causes, based on tide gauge and satellite altimeter data. The sea level all along the coastal region of the Sea of Okhotsk is found to be dominated by the seasonal variation with a maximum in winter and a minimum in summer, which cannot be explained by the annual cycle of atmospheric heat flux and pressure. This sea level variation appears to reflect ocean current variations. Both the Arrested Topographic Waves (ATWs) caused by alongshore wind stress and the Sverdrup transport by wind stress curl show corresponding seasonal variations. Seasonal amplitude of the sea level is relatively large along Sakhalin Island with a tendency of a larger amplitude toward the south. This meridional dependence is consistent with the ATWs, but not with the Sverdrup transport in the Sea of Okhotsk. Seasonal variation of the geostrophic current velocity expected from the sea level variation is comparable to that of the observed nearshore current and is consistent with the theoretical ATW transport. It is also revealed that, on an interannual timescale, the wintertime sea level fluctuates quite coherently all around the Sea of Okhotsk and further along the East Kamchatka and Oyashio coasts in the North Pacific. The altimeter data clearly show that this coherent sea level variation is trapped over the coastal and continental shelf regions with depths shallower than 1000 m. The wintertime sea levels have a higher correlation with the ATW transport than with the Sverdrup transport in the Sea of Okhotsk and the upstream East Kamchatka coast. All these suggest that the interannual sea level variation along the coastal and shelf regions in winter, as well as the seasonal variation, is mainly caused by the ATWs (coastal trapped current forced by the alongshore wind stress). The wintertime

Sverdrup transport, raised by the previous studies, is the secondary contributor to these variations.

38 **1. Introduction**

39

40 The Sea of Okhotsk is a marginal sea located on the northwest rim of the Pacific
41 Ocean, connected through the Kuril Straits (Fig. 1). The surface ocean circulation is
42 mainly characterized by a cyclonic circulation with a western boundary current along
43 the east Sakhalin, which is called the East Sakhalin Current (ESC) (Leonov, 1960; and
44 also reviewed by Talley and Nagata, 1995). The ESC has two velocity cores: one
45 exists near the coast and the other over the shelf slope (Ohshima et al., 2002). The
46 annual mean volume transport of the ESC is estimated as ~7.0 Sv with a large
47 seasonal variation ranging from a maximum of ~12 Sv in winter to a minimum of ~2
48 Sv in summer (Mizuta et al., 2003). The ESC has an important role in southward
49 transport of cold dense shelf water, which is a source water of the North Pacific
50 Intermediate Water (Shcherbina et al., 2004), iron, which is an essential nutrient for
51 phytoplankton (Nishioka et al., 2007), and sea ice (Fukamachi et al., 2009).

52 The driving mechanism of the ESC has been examined in term of the ocean
53 current driven by the wind stress in the Sea of Okhotsk. Simizu and Ohshima (2002)
54 conducted a numerical simulation based on a barotropic ocean model with realistic
55 topography. Their simulation indicates that the nearshore core of the ESC is well
56 explained by the Arrested Topographic Waves (ATWs), which is induced by wind

57 stress along the coast (Csanady, 1978). Ohshima et al. (2004) showed that the
58 Sverdrup balance approximately holds for the cyclonic gyre over the northern
59 half-basin of the Sea of Okhotsk (50°–53°N) and that a major part of the ESC can be
60 regarded as the western boundary current of this gyre. An Ocean General Circulation
61 Model (OGCM) simulation demonstrates that the two velocity cores of the ESC can
62 be reproduced by the wind stress within the Sea of Okhotsk and quantitatively
63 explained by the ATW and Sverdrup transport (Simizu and Ohshima, 2006).

64 Recent studies have suggested that ocean currents in the Sea of Okhotsk are also
65 affected by the subarctic gyre in the North Pacific. Ohshima et al. (2010) showed that
66 the water exchange between the Sea of Okhotsk and the North Pacific predominantly
67 occurs during winter, with inflow through the northern straits and outflow through the
68 southern straits. These features are qualitatively consistent with the Island Rule
69 (Godfrey, 1989). Thus, it is likely that a part of the western boundary current of the
70 subarctic gyre intrudes into the Sea of Okhotsk (Andreev and Shevchenko, 2008;
71 Ohshima et al., 2010). Katsumata and Yasuda (2010) estimated the exchange transport
72 based on the outputs from the OGCM for Earth Simulator (Masumoto et al., 2004)
73 and hydrography in combination, and suggested that the water exchange reaches ~10
74 Sv in winter.

75 The ocean circulation in the Sea of Okhotsk has been also investigated based on
76 sea level variability. Satellite altimeter data have revealed the velocity core structure
77 of the ESC (Ebuchi, 2006) and the annual cycle related to the strength of the
78 anticyclonic circulation in the Kuril Basin (Uchimoto et al., 2008). Itoh and Ohshima
79 (2000) showed that the tide gauge sea level along the northern coast of Hokkaido
80 Island has remarkable seasonal variation, with a peak in winter. They suggested that
81 the wintertime sea level increase is caused by the advent of fresh and cold ESC water.
82 Such a seasonal variation has also been found on the North Pacific side of Hokkaido
83 Island, and the effect of the ESC on the seasonal variation of the Coastal Oyashio was
84 discussed (Isoda et al., 2003; Sakamoto et al., 2013).
85 Along the coast of Hokkaido Island, warm and saline water flows through the
86 shallow Soya Strait as the Soya Warm Current. The Soya Warm Current is a part of
87 the Tsushima Warm Current System in the Sea of Japan and driven by the sea level
88 difference between the Sea of Okhotsk and the Sea of Japan (Aota, 1975; Ohshima,
89 1994; Matsuyama et al., 2006). Therefore, there is a possibility that the sea level
90 fluctuation in the Sea of Okhotsk is related to the strength of the Soya Warm Current
91 and further the Tsushima Warm Current. Tsujino et al. (2008) proposed that the
92 seasonal variability of the Tsushima Warm Current as well as the Soya Warm Current

93 is controlled by the sea level set up by the ATWs along the coast of the Sea of
94 Okhotsk, based on an OGCM simulation and analytical model.

95 In the subarctic North Pacific, it is known that sea level variability along the
96 western coast is well explained by the barotropic response of wind-driven gyre
97 circulation on seasonal to interannual timescales (Isoguchi et al., 1997; Ito et al.,
98 2004; Isoguchi and Kawamura, 2006). Isoguchi and Kawamura (2006) showed that
99 the coastal sea level rises in winter and lowers in summer in accordance with the
100 strength of the East Kamchatka Current (EKC), based on tide gauge and satellite
101 altimeter data. Ito et al. (2004) evaluated the interannual variability of the Oyashio
102 transport by comparing satellite altimeter data with repeated hydrography and
103 mooring observations and found that it is partly explained by the Sverdrup transport.

104 On the other hand, most of the sea surface in the Sea of Okhotsk is covered by
105 sea ice in winter. Therefore, examination of the sea level variability has been limited
106 to seasons with no ice (Ebuchi, 2006) or the southern area (Uchimoto et al., 2008).
107 Examination of the sea level variability over a whole year has been limited to the tide
108 gauge data collected along Hokkaido Island (Konishi et al., 1986; Itoh and Ohshima,
109 2000; Isoda et al., 2003; Andreev and Shevchenko, 2008) and Kuril Islands (Sedaeva
110 and Shevchenko, 2001). Shevchenko and Romanov (2005) analyzed the

111 Topex/Poseidon satellite altimetry data to investigate seasonal changes in the
112 circulation of the Sea of Okhotsk. However, the cause of seasonal and interannual
113 variations of sea level has not yet been fully examined.

114 In this study, we examine tide gauge data mainly provided by the Far Eastern
115 Regional Hydrometeorological Research Institute (FERHRI) and satellite altimeter
116 data to clarify seasonal and interannual variations of the sea level in and around the
117 Sea of Okhotsk. As will be shown, the sea level all along the coastal region of the Sea
118 of Okhotsk shows similar seasonal variation and the coherent variation in winter. This
119 coherent variation extends further into the surrounding coastal areas in the North
120 Pacific. These results imply that the sea level variation in and around the Sea of
121 Okhotsk is related to the ocean current change.

122 The paper is organized in the following manner. Data and methods are described
123 in Section 2. In Section 3, seasonal and interannual variations of the sea level in and
124 around the Sea of Okhotsk are examined based on tide gauge data and satellite
125 altimeter data. The cause of the sea level variation is explored with a focus on the
126 ocean currents related to wind stress change. The relationship between the sea level
127 variation and atmospheric circulation changes is described in Section 4. In Section 5,
128 we discuss the effect of the ocean current change related to the sea level variation on

129 the interannual variability of the sea ice extent in the Sea of Okhotsk. The summary
130 and discussion are presented in Section 6.
131
132 **2. Data and method**
133
134 Tide gauge data were provided by the FERHRI, and the Permanent Service for
135 Mean Sea Level (PSMSL) hosted by the Proudman Oceanographic Laboratory
136 (Woodworth, 1991). These data sets consist of monthly mean sea level records for 15
137 stations in and around the Sea of Okhotsk (Fig. 1 and Table 1). Most of the tide gauge
138 data are available from the 1950s to 1990s. To exclude the effect of the land
139 deformation by the earthquake in the Kuril Straits in 1994 (Lockridge, 1995), we used
140 the tide gauge data before 1993. In the tide gauge data from the FERHRI, there seem
141 to be no significant trends or abrupt changes caused by subsidence and earthquakes.
142 On the other hand, a remarkable increasing trend is found in the tide gauge data for
143 Kushiro provided by the PSMSL. Therefore, we removed this linear trend from the
144 time series for this station. The corrections for the inverse barometer effect caused by
145 changing atmospheric pressure were applied using sea level pressure data from the
146 NCEP/NCAR reanalysis data.
147 Altimeter data used in the present study were derived from the merged products

148 of monthly mean sea surface height anomaly (SSHA) from Topex/Poseidon, Jason-1,
149 and European Research Satellite altimeter observations from 1993 to 2009. The sea
150 level anomalies are produced by the French Archiving, Validation, and Interpolation
151 of Satellite Oceanographic Data (AVISO) project using the mapping method of Ducet
152 et al. (2000). It is known that there is a possibility that the European Research Satellite
153 altimeter observations have an aliasing at the period of one year (Schlax and Chelton,
154 1994). However, the effect of this aliasing problem is expected to be small in and
155 around the Sea of Okhotsk (Uchimoto et al., 2008). The aliased tidal errors in the
156 AVISO altimetry data are relatively large for marginal seas such as the Sea of Okhotsk
157 (e.g., Morimoto, 2009). Significant tidal errors are considered to occur in the
158 northwestern shelf, the Shelikhov Gulf, and the Kuril Straits. For the northwestern
159 shelf and Shelikhov Gulf, we mask out the altimeter data, because sea ice covers these
160 areas in winter. For the Kuril Straits, we do not discuss the results based on the
161 altimeter data.

162 To examine the sea level response to wind forcing, we used ERA-40 data from
163 1958 to 2001 (Uppala et al., 2005). For the Sea of Okhotsk, the high-resolution
164 version with a spatial resolution of 1.125° in latitude and longitude was used. The
165 monthly mean wind stress $\tau = (\tau_x,\tau_y)$ is calculated from 6 hourly wind data based on a

bulk formula as follows:

$$\vec{\tau} = \rho C_D \left|\vec{v}\right| \vec{v} \tag{1}$$

where ρ is the surface air density, C_D is the drag coefficient, and $\vec{v}$ is the wind vector. For C_D, we adopt a stability-independent drag coefficient of Large and Pond (1981) as follows:

$$\begin{aligned} C_D &= 1.2\times10^{-3} && \left|\vec{v}\right| \le 11.0\, m\cdot s^{-1}, \\ C_D &= \left(0.49 + 0.065\left|\vec{v}\right|\right)\times10^{-3} && \left|\vec{v}\right| \ge 11.0\, m\cdot s^{-1}. \end{aligned} \tag{2}$$

For the North Pacific, we used the monthly mean wind stress data with a resolution of 2.5° in latitude and longitude from ERA-40.

In general, the drag coefficient for sea ice is somewhat larger than that for the ocean surface (Lepparanta, 2005). However, it is difficult to evaluate the effect of sea ice on wind stress applied to the ocean, because the ice–water drag coefficient and internal stress in ice cover are also related to the determination of the wind stress. Ohshima and Simizu (2008) showed that a general ocean circulation model with no ice reproduces the velocity field over the east Sakhalin shelf region very well. This result implies that the wind stress applied to the ocean does not change significantly regardless of the presence or absence of sea ice. In this paper, we calculated the wind stress based on a bulk formula for the open ocean without sea ice, even in winter. To assess our results, we also used the monthly mean wind stress data derived from the

184 NCEP/NCAR reanalysis data, in which the roughness of sea ice area is accounted
185 for (Kanamitsu, 1989).

186 In mid- and low-latitude oceans, the sea level variations are dominated by the
187 thermosteric signal caused by seasonal density variations (Gill and Niiler, 1973).
188 Based on previous studies (Gill and Niiler, 1973; Vivier et al., 1999; Qiu, 2002), we
189 evaluated the thermosteric signal caused by local atmospheric heat flux. The
190 thermosteric signal was calculated from net surface heat flux data as follows:

$$\frac{\partial \eta'(t)}{\partial t} = \frac{\alpha}{\rho_o c_p}\left\{Q(t) - \overline{Q(t)}\right\} \tag{3}$$

191

192 where ρ_0 is the reference density, c_p is the specific heat of sea water, and α is the
193 thermal expansion coefficient. The thermal expansion coefficient was calculated from
194 the temperature and salinity averaged over the mixed layer based on the World Ocean
195 Atlas 2005 (WOA05) (Antonov et al., 2006; Locarnini et al., 2006). As the mixed
196 layer depth, we adopted a constant value of 50 m depth which corresponds to the
197 typical seasonal thermocline depth in the Sea of Okhotsk (Ohshima et al., 2005). $Q(t)$
198 is the net surface heat flux derived from the climatological monthly means of the
199 NCEP/NCAR reanalysis data during 1979 to 2008. The overbar denotes the annual
200 average of the climatological monthly means from January to December. The
201 estimated thermosteric values nearest to the tide gauge stations and satellite altimeter

202 gridded point were used for evaluation of the thermosteric component for the
203 corresponding sea level data.

204

205 **3. Results**

206

207 We begin by showing the time series of raw monthly mean data from the tide
208 gauges averaged over the Sakhalin coast (Fig. 2). We found a seasonal cycle with a
209 clear maximum in winter and a minimum in summer. The timing of this seasonal
210 cycle is out of phase with that of the altimeter SSH over the Kuril Basin (Uchimoto et
211 al., 2008) and the North Pacific (e.g., Stammer, 1997). The interannual variability also
212 has a large fraction on the sea level variability. For example, the wintertime peak of
213 22 cm in 1973/1974 season is about twice larger than that of 1972/1973 season. Below,
214 we will examine the seasonal and interannual sea level variations individually.

215

216 *3.1. Seasonal variation*

217

218 To examine the seasonal variation of the sea level, the climatological monthly
219 mean was calculated for each tide gauge. Figure 3a shows the annual cycle of the sea
220 level at each tide gauge. The most remarkable feature is the peak in December or

January. This annual cycle is still evident after the thermosteric signal and inverse barometer effect is removed from each tide gauge data (Fig. 3b). In addition to the wintertime peak, the sea level along the northern coast of Hokkaido Island (K–O) and the northern shelf of the Sea of Okhotsk (B, C) have a secondary peak in September (Fig. 3a). The secondary peak for the northern coast of Hokkaido Island is explained by the seasonal variation of the Soya Warm Current (Itoh and Ohshima, 2000). On the other hand, the secondary peak for the northern shelf might be related to the halosteric component, because a relatively large river discharge occurs in summer near these tide gauges (M, N) (e.g., Dai and Trenberth, 2002). Hereafter, the thermosteric and inverse barometer effects are subtracted from the tide gauge data.

Next, we examined the spatial distribution of the seasonal amplitude with the winter peak, using both the tide gauge and satellite altimeter data. Considering that most of the tide gauge data show maximum peaks from December to January and minimum peaks from April to May (Fig. 3b), and that satellite altimeter data cannot be used in the sea-ice covered season, the sea level difference between December and May is adopted as a measure of the seasonal amplitude. The tide gauge data (Fig. 4a) show that the seasonal amplitude is relatively large along Sakhalin Island (E, G, H, I, J), with the difference value larger than 10 cm. This result is consistent with the

239 satellite altimeter data (Fig. 4b). On the other hand, the seasonal amplitude is much
240 smaller in the basin with depths greater than 1,000 m (see the depth contours in Fig.
241 1), indicating that the seasonal variation is confined to the coastal and shelf regions.
242 Since the seasonal variation of sea level in and around the Sea of Okhotsk is not
243 explained by the thermosteric height signal at all (Fig. 3b), the variation is suggested
244 to be related to dynamic response of the ocean current systems. Considering that the
245 high sea level season (winter) corresponds to the strong wind season and that the
246 seasonal amplitude is relatively large along the western boundary current region off
247 Sakhalin Island, the seasonal variation is likely caused by near-barotropically quick
248 responses through the ATWs and/or the western boundary current through the
249 Sverdrup transport (e.g., Ebuchi, 2006; Simizu and Ohshima, 2006). In winter,
250 northwesterly and northeasterly winds prevail over the western part of the Sea of
251 Okhotsk and the eastern part of the East Kamchatka Peninsula, respectively (Fig. 5a).
252 This wind pattern is favorable for the pile up of the Ekman transport to set up the
253 ATWs and the sea level rise along these coastal regions. In the western subarctic gyre
254 of the North Pacific, it has been suggested that the sea level along the western coast
255 increases in winter by intensification of the southward western boundary current
256 through the time-varying Sverdrup balance (Isoguchi and Kawamura, 2006). Similarly,

257 the southward ESC in the Sea of Okhotsk also intensifies in winter (Mizuta et al.,
258 2003; Simizu and Ohshima, 2006). These results imply that the coastal sea level along
259 Sakhalin Island also may be affected by the compensation of the sea level change in
260 the offshore through the Sverdrup balance (Fig. 5b).

261 Therefore, we here examine the effects of ATW and Sverdrup transport on
262 seasonal sea level variations along Sakhalin Island. According to Csanady (1978), the
263 alongshore volume transport of the ATWs that occurs in a steady manner, V_{ATW}, is
264 determined by:

$$V_{ATW} = \int_{l_1}^{l_2} \frac{\tau_l}{\rho f} dl, \tag{4}$$

265

266 where a right-handed coordinate system is used with the l axis along the coastline. τ_l is
267 the alongshore component of the wind stress, ρ is the density of water, and f is the
268 Coriolis parameter. On timescales larger than a month, the volume transport of the
269 coastally trapped flow is determined by Eq. (4), which can be derived from the linear
270 momentum equation (or vorticity equation) in a stationary state. This steady flow is
271 called the Arrested Topographic Waves (ATWs) by Csanady [1978]. A similar
272 equation was also used to examine the coastal sea level along the Alaska/Canada coast
273 (Qiu, 2002). This equation implies that the alongshore transport at l_1 is the sum of the
274 Ekman transport to or from the coast over the integral route from the starting point of

275 l_2 to l_1. The integral route of the Ekman transport depends on several factors, such as
276 the shape of the coastline, shelf width, shelf slope, and bottom friction, which are
277 difficult to identify (Csanady, 1978). The OGCM simulation of the Sea of Okhotsk
278 indicates that the starting point of the integral route suitable for the ATW calculation
279 is the west of the Shelikhov Gulf (Fig. 1) (Simizu and Ohshima, 2002). However, the
280 effect of wind stress variability in the North Pacific was not included in their model
281 simulation. Since similar seasonal variations of the sea level are also found along the
282 northern coast of the Sea of Okhotsk and the eastern coast of the Kamchatka
283 Peninsula (Fig. 4), there is a possibility that the ATWs along Sakhalin Island is also
284 affected by wind stress over further upstream regions. Thus, we examine two
285 additional integral routes (routes 2 and 3, Fig. 5c) as well as the one (route 1)
286 proposed by Simizu and Ohshima (2002).

287 The Sverdrup transport in the Sea of Okhotsk (V_s) is estimated based on the
288 following equation:

289 $$V_S = -\frac{1}{\beta\rho}\int_{x_1}^{x_2} curl\vec{\tau}dx, \quad (5)$$

290 where the right-handed Cartesian coordinate system is adopted with x and y axes in
291 the eastward and northward directions, respectively. β is the y derivative of the
292 Coriolis parameter and $\vec{\tau}$ is a wind stress vector. The integral route is taken along

293 latitudinal lines from the eastern boundary (x_2) to the western boundary (x_1), where
294 the eastern boundary is defined as the west coast of the Kamchatka Peninsula and the
295 Kuril Islands (Fig. 5b). Northward Sverdrup transport is defined as positive. Several
296 studies imply that a part of the EKC intrudes into the Sea of Okhotsk through the
297 northern part of the Kuril Straits and that the inflow is significantly correlated with the
298 Sverdrup transport in the North Pacific (Andreev and Shevchenko, 2008; Ohshima et
299 al., 2010). To evaluate the variability of the inflowing water from the Pacific, we also
300 examined the Sverdrup transport over the North Pacific, integrated from the eastern
301 boundary of the North Pacific. The Sverdrup transport in each basin is meridionally
302 averaged over 46°–50°N.

303 Figure 6 compares the seasonal variation of the sea level along Sakhalin Island
304 with that of the ATW transport and Sverdrup transport. As the representative for the
305 sea level, we show the climatological monthly values averaged over 6 tide gauge
306 stations (D–J) (Fig. 6a). For the ATW, the climatological values from 1979 to 2008 for
307 routes 1, 2, and 3 are shown (Fig. 6b). For the Sverdrup transport, the climatological
308 values for both the Sea of Okhotsk and the North Pacific are shown (Fig. 6c). Both the
309 ATW transport and Sverdrup transport show a maximum from December to January
310 and a minimum from June to August, although the absolute value of the volume

311 transport is rather different among these transports. These seasonal variations are also
312 similar to those of the sea level along Sakhalin Island. Similar results are obtained
313 using the NCEP/NCAR reanalysis data, although the seasonal amplitude of the ATW
314 transport calculated using the NCEP/NCAR reanalysis data is somewhat larger than
315 that using the ERA-40 data (not shown).

316 Next, we compare the latitudinal dependence of the seasonal sea level variation
317 from 46° to 52°N with those of the corresponding ATW transport and Sverdrup
318 transport. The ATW transport at each latitude is calculated based on the wind stress
319 along route 1. The seasonal amplitude is evaluated from the difference of the
320 climatological value between December and May. The seasonal amplitude of the sea
321 level tends to be larger in lower latitudes (Fig. 7a). This latitudinal dependence is
322 consistent with that of the ATW (Fig. 7b). The larger seasonal variation of the ATW in
323 the southern areas is caused by the prevailing southward wind along Sakhalin Island
324 in winter (Fig. 5a). On the other hand, the latitudinal dependence of the Sverdrup
325 transport in the Sea of Okhotsk is contrary to that of the sea level. The latitudinal
326 dependence of the seasonal sea level variation is not qualitatively explained by the
327 Sverdrup transport.

328 The above analyses suggest that the seasonal variation of the sea level along

329 Sakhalin Island is dominated by the ATWs. To quantify this suggestion, we evaluated
330 the geostrophic current from the sea level data and compare it with the current
331 velocity data obtained from mooring measurements (Mizuta et al., 2004) and the
332 theoretical ATW transport. Assuming that the seasonal current variation is barotropic,
333 the seasonal amplitude of the geostrophic current speed Δv is calculated as follows:

$$\Delta \mathrm{v} = \frac{g}{f} \cdot \frac{\Delta(\eta_{\mathrm{c}} - \eta_{0})}{\Delta \mathrm{x}} \tag{6}$$

334

335 where Δx is the width of the ATW, g is gravity acceleration (9.8 m s^{-2}), f is the Coriolis
336 parameter (1.2×10^{-4} s^{-1}), and $\Delta(\eta_c - \eta_o)$ is the seasonal amplitude of the sea level
337 difference between the coast and the offshore, where the offshore sea level is assumed
338 to be constant.

339 Based on the observed current structure from the surface drifters (Ohshima et al.,
340 2002) and the simulated result of the nearshore branch of the ESC using an OGCM
341 (Simizu and Ohshima, 2006), the width of the ATW Δx is assumed to be ~70 km.
342 Since the difference between the monthly mean sea levels along Sakhalin Island in
343 January and April is about 14 cm (Fig. 6a), the seasonal amplitude of the surface
344 velocity Δv would be ~16 cm s^{-1} according to the geostrophic balance (Eq. 6). Since
345 the monthly mean velocity obtained from the mooring measurement at 53°N showed
346 that the difference between the southward current velocity near the coast in January

347 and April is ~20 cm s^{-1} (Fig. 6 of Mizuta et al., 2003), the seasonal amplitude of the
348 estimated value is comparable to the observed value.

349 When the thickness H of the ATW is assumed to be 100 m, which is the mean
350 water depth over the width of the ATW (from the coast to 70 km offshore in latitudes
351 of 46°–52°N), the seasonal variation of the volume transport ($\Delta v \times H \times \Delta x$) is
352 estimated to be ~1.3 Sv using the velocity difference (Δv = 20 cm s^{-1}) measured from
353 the moorings. The seasonal variation of the theoretical ATW transport calculated using
354 the wind stress along routes 1, 2, and 3 is 0.95 (1.6), 0.85 (1.2), and 2.5 (3.0) Sv,
355 respectively (The brackets show the theoretical ATW transport for the same routes
356 calculated using the NCEP/NCAR reanalysis data). Hence, the orders of the
357 theoretical values are comparable to the estimated values.

358 We also evaluate the contribution of the offshore (western boundary current)
359 component of the ESC to the seasonal sea level variation. From the vertical cross
360 sections of the monthly mean velocity field obtained from the mooring measurement
361 (Mizuta et al., 2003), the southward current speed of the offshore component at the
362 surface is ~25 cm s^{-1} and ~15 cm s^{-1} in January and April, respectively. Since the
363 zonal width of the offshore ESC component is ~50 km (Mizuta et al., 2003), the sea
364 level rise toward the coast by this current is estimated to be ~15 cm and ~9 cm in

365 January and April, respectively. Since the difference between the estimated sea level
366 in January and April (6 cm) is smaller than that of the observed sea level difference
367 (14 cm), the seasonal variation of the sea level is insufficiently explained by the
368 Sverdrup transport. As well as the latitudinal dependence of the seasonal amplitude,
369 these comparisons on the basis of the geostrophic balance imply that the ATWs are the
370 primary contributor to the seasonal sea level variation and that the Sverdrup transport
371 is the secondary.

372

373 *3.2. Interannual variation*

374

375 In this section, we examine the interannual variability of the sea level, compared
376 to those of ATW and Sverdrup transports. For the examination of the interannual
377 variation, the climatological seasonal variation was removed from the tide gauge and
378 satellite altimeter data. The standard deviations of the monthly sea level anomalies in
379 winter (December to February) are considerably larger than those in the other seasons
380 (not shown). Wind speed and its interannual variability, a likely cause of the sea level
381 variation, are also large in winter. Thus, we mainly focus on the interannual variability
382 in winter. In this paper, the year of the wintertime from December 1969 to February
383 1970 is defined as 1970, and similarly for the other years. Figure 8 shows the time

384 series of the wintertime tide gauge sea level anomalies from the East Kamchatka coast
385 (A), then all around the Okhotsk coast (B–N), and finally to the Oyashio coast (O).
386 We found that the wintertime sea levels fluctuate quite coherently all around the Sea
387 of Okhotsk (B–N) with a remarkable year-to-year variability: positive anomalies in
388 1970, 1974, 1981, and 1984 and negative anomalies in 1972, 1979, and 1982. It
389 should be noted that these coherent variations partly extend upstream to the East
390 Kamchatka coast (A) and downstream to the Oyashio coast (O).

391 To extract dominant modes for the interannual variability of tide gauge sea levels
392 in and around the Sea of Okhotsk, Empirical Orthogonal Function (EOF) analysis
393 based on a covariance matrix was applied to sea level data from 11 stations (A, B, E,
394 G, H, I, J, L, M, N, and O) at which continuous data were obtained from 1965 to 1988.
395 The first EOF mode for the wintertime sea level anomalies explains 61% of the total
396 variance, indicating that this mode is by far the dominant mode. The temporal
397 coefficient of the first EOF mode (PC-1) is shown at the bottom of Fig. 8. The spatial
398 structure of the first EOF mode shows all positive values with large values along
399 Sakhalin Island (Fig. 9a).

400 The interannual variability of the wintertime sea level is further examined using
401 satellite altimeter data. We used the SSHA averaged in December, because the

altimeter data are not fully available for the sea ice seasons from January to February. Figure 9b shows the regression map of the SSHAs onto the time series of the normalized SSHAs for the Sakhalin coast (48°–49°N, 143°–144°E). The significant positive correlations are found all over the shelf region with the water depths shallower than 1,000 m in the Sea of Okhotsk (Fig. 1). The significant correlations are also found further to the eastern shelf of the Kamchatka Peninsula and the Oyashio coast in the North Pacific. The absolute values of the regression coefficients in these regions are comparable to those for the tide gauge data.

To explore the mechanism giving rise to the coherent sea level variation, we compared the interannual variability of the wintertime sea level along Sakhalin Island with those of the ATW and Sverdrup transports. As an index of the sea level along Sakhalin Island, we used the tide gauge data averaged over stations E, G, H, I, and J, which is found to be quite similar to the PC-1 (the correlation between them is 0.98). Table 2 summarizes the correlation coefficients between the sea level along Sakhalin Island and the related volume transports. The wintertime sea level is significantly correlated with both the ATW and Sverdrup transports in the Sea of Okhotsk, and the former is larger than the latter. The result that the sea level has a higher correlation with the ATW1 (ATW for route 1) than the ATW2, supports that the integral route

420 proposed by Simizu and Ohshima (2002) is reasonable. Figure 10 shows the time
421 series of the sea level anomalies and the ATW anomalies for route 1, demonstrating
422 their good correspondence all through the analyzed period. It is noteworthy that the
423 correlation between the sea level and ATWs for route 3 is also high (Table 2). The
424 wind stress far from the east of Kamchatka and the Bering Sea may also contribute to
425 the ATWs in the Sea of Okhotsk to some extent. Similar results are obtained using the
426 NCEP/NCAR reanalysis data (Table 2).

427 Finally, we examine the relationship between the sea level and the ATWs all
428 through the seasons. In Fig. 2, the time series of the monthly mean ATW transport for
429 route 1 is superimposed on the sea level data. The timing and strength of the peaks of
430 the ATW transport corresponds to those of the sea level anomalies. The correlation
431 coefficients between the monthly mean of the sea level and the ATWs for routes 1 and
432 3 are 0.60 and 0.56 (significant at 95% confidence level), respectively. The
433 correlations between the sea level and ATWs from spring to autumn are quite small
434 and insignificant (Table 3). Since the variance of the wind stress in these seasons is
435 smaller than that in winter, it is likely that the contributions of other factors rather than
436 the ATWs are relatively large from spring to autumn, when compared to the winter
437 case.

438

439 *3.3. The sea level variation in the North Pacific and its relation to the ATWs*

440

441 For the North Pacific, Isoguchi and Kawamura (2006) examined the relationship

442 between the coastal sea level along the Kamchatka Peninsula and the Sverdrup

443 transport over the North Pacific and found the significant correlation between them on

444 seasonal to interannual timescales. Ito et al. (2004) also indicated that year-to-year

445 variability of the Oyashio transport is partly explained by the time-varying Sverdrup

446 transport. The present study suggests that the coherent sea level variation in the Sea of

447 Okhotsk extends to the coastal regions in the upstream EKC and the downstream

448 Oyashio on seasonal (Fig. 4) to interannual timescales (Fig. 10). Thus, we here

449 examine the effect of the ATWs on the sea level variability in these western boundary

450 current regions of the North Pacific.

451 As for the sea level data at the EKC and Oyashio regions, we use the tide gauge

452 sea level data at Petropavlovsk–Kamchatsky (PK) and Kushiro (Fig. 1) from 1958 to

453 2001. The integral routes for the ATWs to PK and Kushiro are determined as the paths

454 from starting points 3 and 1 to the locations of the tide gauges, respectively (Fig. 5c).

455 We conducted a correlation analysis between the sea level in winter and the ATWs and

456 compare it with that for the Sverdrup transport in the North Pacific.

457 The correlation coefficients among the sea levels and the transports are
458 summarized in Table 4. The sea level at PK is highly correlated with the
459 corresponding ATWs (r = 0.65) rather than the Sverdrup transport (r = 0.59),
460 suggesting that the ATWs primarily contributes to the sea level variation. For Kushiro,
461 the sea level is significantly correlated with both the ATW transport (r = 0.59) and
462 Sverdrup transport (r = 0.56) and their correlation coefficients are comparable. It is
463 noted that there is no significant correlation between the ATW transport and Sverdrup
464 transport (r = 0.15), suggesting that the sea level is affected by both transports. When
465 we built a statistical regression model for the sea level at Kushiro based on both the
466 ATW and Sverdrup transports, the multiple correlation coefficient between the
467 observed and predicted sea level becomes a significantly high value of 0.76.
468
469 **4. Atmospheric circulation variability**
470
471 To understand the wintertime atmospheric circulation pattern related to the
472 coherent sea level variation, we performed regression analyses of wind stress, wind
473 stress curl, and sea level pressure onto the PC-1 of the tide gauge sea level in winter
474 (December to February). Monthly sea level pressure and wind stress data in the
475 northern hemisphere were used from the NCEP/NCAR reanalysis data. Figure 11a

476 shows the regression map of the wind stress over the North Pacific onto the PC-1. The
477 northeasterly wind anomalies are found over the Sea of Okhotsk and the Bering Sea.
478 These wind stress anomalies induce Ekman transport anomalies over the coastal
479 region to pile up the sea level along Sakhalin Island and the east coast of the
480 Kamchatka Peninsula to generate the ATWs. The PC-1 is also significantly correlated
481 with the wind stress curl over the Sea of Okhotsk (Fig. 11b). This result indicates that
482 the northeasterly wind anomalies lead to the increase in both the ATW transport and
483 Sverdrup transport in the Sea of Okhotsk.

484 From the regression map of the sea level pressure, the northeasterly wind
485 anomalies related to the PC-1 are also found to be related to the dipole pattern of the
486 high pressure over the Eurasian continent and the low pressure over the subtropics
487 (Fig. 11c). This anomalous sea level pressure pattern resembles the negative phase of
488 the Western Pacific (WP) pattern dominated over the northern hemisphere (Horel and
489 Wallace, 1981) and the strengthened Aleutian low.

490 We thus calculated the correlations between the PC-1 and the WP index of the
491 Climate Prediction Center (Barnston and Livezey, 1987) as well as the North Pacific
492 Index (NPI). The NPI is an index of Aleutian low strength and is defined as the sea
493 level pressure averaged over a region from 30°–60°N and 160°E–140°W (Trenberth

494 and Hurrell, 1994). The significant negative correlation between the PC-1 and the WP
495 index is obtained (r = -0.46) at 90% confidence level, when we use the WP index in
496 January. The PC-1 has a significant correlation with the NPI in December (r = -0.60)
497 at 95% confidence level. Thus, when the WP pattern is in the negative phase and the
498 Aleutian low is strengthened, the sea level in and around the Sea of Okhotsk is piled
499 up coherently, mainly associated with strengthened ATWs.
500

501 **5. Relation to sea ice extent variability**
502

503 It is known that the southward transport of the ESC has a role on the southward
504 transport of the sea ice extent within the Sea of Okhotsk (Fukamachi et al., 2009). The
505 current along Sakhalin Island associated with the coherent sea level pile-up may lead
506 to the southward extension of the sea ice. Conversely, the current along the
507 Kamchatka Peninsula associated with the sea level pile-up may suppress the sea ice
508 extent through the inflow of warmer water from the Pacific. The importance of the
509 ocean thermal condition in the East Kamchatka Current on the interannual variability
510 of the sea ice extent in February to March has been suggested (Nakanowatari et al.,
511 2010).

512 We now examine the relationship between the sea ice extent variability and the

513 PC-1 of the sea level in winter, assuming that the ocean current affects the sea ice
514 extent. We use the sea ice concentration data from 1971 to 2006 provided from the
515 Japan Meteorological Agency (JMA). These data are a merged product from various
516 sources of observations, including visual and aircraft observations as well as satellite
517 observations of infrared, visible, and microwave radiometers.

518 Based on the correlation analysis between the monthly sea ice extent averaged
519 over the Sea of Okhotsk and the PC-1 (sea level during December to February) from
520 1971 to 1988, the PC-1 has by far the highest negative correlation with the sea ice
521 extent in January (r = -0.67, significant at 95% confidence level based on the Monte
522 Carlo simulation). As also shown in the time series (Fig. 12), less ice extent
523 corresponds well with larger PC-1 implying stronger currents. The PC-1 based on
524 the sea level data from December to January is still significantly correlated with the
525 sea ice extent in January (r=-0.69). Conversely, the correlations between the PC-1 and
526 the sea ice extent in December and February are only -0.01 and -0.32, respectively.

527 In December, the sea ice extent variability has been reported to be mostly
528 determined by the local heat flux over the northwestern area in the preceding autumn
529 (October–November) (Ohshima et al., 2006; Sasaki et al., 2007). In February to
530 March, the ocean thermal condition inflowing from the Pacific is also a determinant

531 factor for the sea ice extent as well (Nakanowatari et al., 2010). Our result implies that
532 for January, the warmer coastal current from the Pacific, associated with the sea level
533 pile-up, suppresses the sea ice extent dynamically and/or thermodynamically.
534
535
536 **6. Summary and discussion**
537
538 The cause of the sea level variability in the Sea of Okhotsk had previously been
539 investigated mostly in terms of the relation to wind-driven ocean circulation (Ebuchi,
540 2006; Andreev and Shevchenko, 2008). Using satellite altimeter data, Ebuchi (2006)
541 indicated that the seasonal to interannual variability of the ESC is related to both the
542 ATWs caused by alongshore wind stress and the Sverdrup transport by wind stress
543 curl. However, these previous studies were based on altimeter data in no sea ice
544 seasons or tide gauge data only in the southern part of the Sea of Okhotsk. The sea
545 level variability over the entire Sea of Okhotsk for the full annual cycle had not yet
546 been examined. In this study, using tide gauge data in and around the Sea of Okhotsk
547 and satellite altimeter data, we examined the seasonal and interannual variations of the
548 sea level and their causes in terms of both the thermosteric signal and wind-driven
549 ocean circulation.

550 In and around the Sea of Okhotsk, the sea level along the coastal region is found
551 to be dominated by the seasonal variation with a maximum in winter and a minimum
552 in summer. Since this seasonal variation is not explained by the annual heat flux cycle
553 and inverse barometer effect caused by changing atmospheric pressure, the cause for
554 the seasonal variation is explored in terms of the ATW and Sverdrup transports. We
555 found that both transports show the corresponding seasonal variation. The seasonal
556 amplitude of the sea level is relatively large along Sakhalin Island with a tendency of
557 larger amplitudes toward the south. This meridional dependence of the seasonal
558 variation is consistent with the ATWs but not with the Sverdrup transport in the Sea of
559 Okhotsk. The seasonal amplitudes of the geostrophic current speed of the nearshore
560 ESC and the associated volume transport estimated from the observed sea level data
561 are ~16 cm s^{-1} and ~1.3 Sv, respectively. These values are quantitatively comparable
562 to the observed amplitude of the current speed (~20 cm s^{-1}) and the theoretical ATW
563 transport (~1 Sv). While the Sverdrup transport partly explains the seasonal sea level
564 variation, its contribution is smaller than that of the ATWs.
565 On an interannual timescale, it is also revealed that the wintertime sea levels
566 fluctuate quite coherently along the coastal and shelf regions in the Sea of Okhotsk
567 and further along the East Kamchatka and Oyashio coasts in the North Pacific. The

568 first EOF mode of the wintertime sea level explains 61% of the total variance with a
569 large amplitude along Sakhalin Island. Satellite altimeter data support these results
570 and clearly reveal that the coherent sea level variation is trapped over the continental
571 shelf (Fig. 9b). Wintertime sea level along Sakhalin Island has a higher correlation
572 with the ATW transport than with the Sverdrup transport. On the other hand, the
573 significant correlation between the sea level along Sakhalin Island and the ATWs is
574 not found from spring to autumn. These findings imply that the interannual sea level
575 variation along the coastal and shelf regions in the Sea of Okhotsk in winter, as well
576 as the seasonal variation, is mainly caused by the ATWs (coastal trapped currents
577 forced by alongshore wind stress). The wintertime Sverdrup transport, raised by the
578 previous studies, seems to be a secondary factor.

579 The present study also showed that the sea levels along the upstream East
580 Kamchatka coast and the downstream Oyashio coast coherently vary with the sea
581 level around the Sea of Okhotsk on seasonal to interannual timescales and that these
582 variations have higher correlation with the ATWs than with the Sverdrup transports.
583 The importance of the wind stress along the coast on the sea level variability was
584 pointed out only by a numerical study (Tatebe and Yasuda, 2005). The present study
585 raises the caution about the previous studies that the coastal sea level variability is

586 determined by the Sverdrup transport.

587 It is known that the ESC transport and its variability is mainly governed by the
588 Sverdrup transport (Ohshima et al., 2004; Simizu and Ohshima, 2006). Conversely,
589 this study suggests that the coastal sea level variability is primarily explained by the
590 ATWs. The ATWs have a shallow structure and are trapped over the nearshore region,
591 while the western boundary current exists offshore with a deeper structure. Therefore,
592 the coastal sea level can be largely governed by the ATWs, despite that the ATW
593 transport is one order less than the Sverdrup transport. Our results are consistent with
594 the previous numerical study (Shimada et al., 2005), which showed that the shelf
595 region has a role of an obstacle on the intrusion of the barotropic response in the
596 central basin. Since the northeasterly wind stress anomaly (Fig. 11a) is accompanied
597 by the strengthened wind stress curl in the Sea of Okhotsk, a part of the correlation
598 between the sea level and Sverdrup transport might be an apparent one.

599 Using an OGCM and analytical models, Tsujino et al. (2008) proposed that the
600 ATWs are responsible for the seasonal variations of the throughflow transport of the
601 Japan Sea. Wintertime wind stress along the coastal region of the Sea of Okhotsk
602 yields the positive SSHAs and the following SSH rise weakens the Tsushima Warm
603 Current as well as the Soya Warm Current in winter. Our result that the seasonal sea

604 level variation in the Sea of Okhotsk is dominated by the ATWs supports their study.
605 We also found that the interannual variation of the coastal sea level in winter is well
606 explained by the ATWs. According to Ebuchi et al. (2009) and Fukamachi et al.
607 (2010), the Soya Warm Current exhibits interannual variability even in winter,
608 although the average transport is small in winter. Therefore, we would like to propose
609 that the ATWs (i.e., alongshore wind stress) partly control these throughflow
610 transports on an interannual timescale as well as seasonal timescale.

611 In this study, the ATWs are assumed to be barotropic for simplicity, on the basis
612 of Csanady (1978). Even if the effect of stratification is taken into account, our results
613 would not be essentially changed. Since the ATWs could have a partially baroclinic
614 structure analogous to the coastally trapped waves (CTWs) that have a hybrid
615 structure of barotropic shelf waves and internal Kelvin waves, it is likely that the
616 ATWs are somewhat accompanied by the dynamical displacement of isopycnals.
617 Actually, Mizuta et al. (2004) showed that the alongshore component of wind stress is
618 essential for the interannual variability of the isopycnals in the southern part of the
619 Sea of Okhotsk in winter. Considering that the subinertial variability of velocity in the
620 ESC over the continental shelf is dominated by CTWs and its vertical structure is
621 fairly barotropic (Mizuta et al., 2005), it is expected that the vertical structure of the

622 ATWs in the Sea of Okhotsk is also fairly barotropic, while that the coherent sea level
623 variation is partly or slightly accompanied by the displacement of isopycnals.

624 Previous studies suggest that wintertime increases in the sea level along the
625 Okhotsk coast of Hokkaido (Itoh and Ohshima, 2000) and the Oyashio coast (Isoda et
626 al., 2003) are related to the advent of lighter ESC water from the upstream region. In
627 fact, sea surface salinity reductions are observed along Sakhalin Island (~50° N) in
628 autumn (Shevchenko and Chastikov, 2008). From the current velocity data of the ESC,
629 the Amur River discharge in May is estimated to arrive at the coast of Sakhalin Island
630 (~50° N) by October (Mizuta et al., 2003). When we carefully see Fig. 3b, it seems
631 that the tide gauge sea level near the Amur River (D) begin to rise in September to
632 October (Fig. 3b). Thus, a portion of the sea level rise along Sakhalin Island in
633 autumn–winter may be related to advection of low-salinity water from the Amur
634 River.

635 With respect to the interannual variability, we also examine the effect of the
636 advent of lighter ESC water from the upstream region on the sea level fluctuation
637 using the tide gauge data. The wintertime peak is commonly found in December along
638 Sakhalin Island (Fig. 6a) and the Okhotsk coast of Hokkaido (L, Fig. 3b). While, the
639 timing of the peak along the Oyashio coast in January is one month behind that along

640 Sakhalin Island in December. Thus, we calculated the lead-lag correlations between
641 the monthly sea level anomalies among all these tide gauges during winter (from
642 November to March). Significant correlations are obtained only for no time lag, and
643 we could not find any significant correlations when the sea level along Sakhalin
644 Island leads those at the downstream stations by one or two months. Thus, the effect
645 of the advent of cold and fresh water is considered to be smaller than that of the
646 dynamical displacement in the southern part of the Sea of Okhotsk on the interannual
647 timescale.
648
649 **Acknowledgments**
650
651 Tide gauge data around the Sea of Okhotsk were provided by the Far Eastern
652 Regional Hydrometeorological Research Institute. Some figures were produced with
653 the GrADS package developed by B. Doty. The altimeter products were produced by
654 SSALTO/DUACS and distributed by AVISO with support from CNES. We wish to
655 thank N. Ebuchi for his constructive discussion and anonymous reviewers for their
656 constructive comments. This work was supported by a fund from Core Research for
657 Evolution Science and Technology (CREST), Japan Science and Technology

658 Corporation (JST), Grant-in-Aid for Scientific Research (20221001, 22221001).

659 **References**

660

661 Andreev, A.G., Shevchenko, G.V., 2008. Interannual variability of water transport by
662 the East Kamchatka and East Sakhalin Currents and their influence on dissolved
663 oxygen concentration in the Sea of Okhotsk and subarctic Pacific. Russian
664 Meteorology and Hydrology, 33, 657-664 (in English).
665 Antonov, J.I., Locarnini, R.A., Boyer, T.P., Mishonov, A.V., Garcia, H.E., 2006. World
666 Ocean Atlas 2005, vol.2, Salinity, NOAA Atlas NESDIS 62, 182 pp., NOAA,
667 Silver Spring, Md.
668 Aota, M., 1975. Studies on the Soya Warm Current. Teion Kagaku, 33, 151-172 (in
669 Japanese).
670 Barnston, A.G., Livezey, R. E., 1987. Classification, seasonality and persistence of
671 low-frequency atmospheric circulation patterns. Monthly Weather Review, 115,
672 1083-1126.
673 Csanady, G.T., 1978. The arrested topography wave. Journal of Physical
674 Oceanography, 8, 47-62.
675 Dai, A., Trenberth, K.E., 2002. Estimates of freshwater discharge from continents:
676 Latitudinal and seasonal variations. Journal of Hydrometeorology, 3, 660-687.
677 Ducet, N., Le Traon, P.Y., Reverdin, G., 2000. Global high-resolution mapping of
678 ocean circulation from TOPEX/Poseidon and ERS-1 and -2. Journal of
679 Geophysical Research, 105, 19,477-19,498.
680 Ebuchi, N., 2006, Seasonal and interannual variations in the East Sakhalin Current
681 revealed by TOPEX/POSEIDON altimeter data. Journal of Oceanography, 62,
682 171-183.

683 Ebuchi, N., Fukamachi, Y., Ohshima, K.I., Shirasawa, K., Ishikawa, M., Takatsuka, T.,
684 Daibo, T., Wakatsuchi, M., 2006. Observation of the Soya Warm Current using
685 HF ocean radar. Journal of Oceanography, 61, 47-61.
686 Ebuchi, N., Fukamachi, Y., Ohshima, K. I., Wakatsuchi, M., 2009. Subinertial and
687 seasonal variations in the Soya Warm Current revealed by HF ocean radars,
688 coastal tide gauges, and bottom-mounted ADCP. Journal of Oceanography, 65,
689 31-43.
690 Fukamachi, Y., Shirasawa, K., Polomoshnov, A.M., Ohshima, K.I., Kalinin, E.,
691 Nihashi, S., Melling, H., Mizuta, G., Wakatsuchi, M., 2009. Direct observations
692 of sea-ice thickness and brine rejection off Sakhalin in the Sea of Okhotsk.
693 Continental Shelf Research, 29, 1541-1548.
694 Fukamachi, Y., Ohshima, K. I., Ebuchi, N., Bando, T., Ono, K., Sano, M., 2010.
695 Volume transport in the Soya Strait during 2006-2008. Journal of Oceanography,
696 66, 685-696.
697 Gill, A.E., Niiler, P.P., 1973. The theory of the seasonal variability in the ocean. Deep
698 Sea Research, 20, 141-177.
699 Godfrey, J.S., 1989. A Sverdrup model of the depth-integrated flow for the world
700 ocean allowing for island circulations. Geophysical and Astrophysical Fluid
701 Dynamics, 45, 89-112.
702 Horel, J.D., Wallace, J.M., 1981. Planetary-scale atmospheric phenomena associated
703 with the Southern Oscillation. Monthly Weather Review, 109, 813-829.
704 Isoguchi, O., Kawamura, H., Kono, T., 1997. A study on wind-driven circulation in
705 the subarctic North Pacific using TOPEX/POSEIDON altimeter data. Journal of
706 Geophysical Research, 102, 12,457-12,468.

Isoguchi, O., Kawamura, H., 2006. Seasonal to interannual variations of the western boundary current of the subarctic North Pacific by a combination of the altimeter and tide gauge sea levels. Journal of Geophysical Research, 111, C04013, doi:10.1029/2005JC003080.

Isoda, Y., Kuroda, H., Myousyo, T., Honda, S., 2003. Hydrographic feature of coastal Oyashio and its seasonal variation. Bulletin on Coastal Oceanography, 41, 5-12 (in Japanese with English abstract).

Ito, S., Uehara, K., Miyao, T., Miyake, H., Yasuda, I., Watanabe, T., Shimizu, Y., 2004. Characteristics of SSH anomaly based on TOPEX/POSEIDON altimeter and in situ measured velocity and transport of Oyashio on OICE. Journal of Oceanography, 60, 425-437.

Itoh, M., Ohshima, K.I., 2000. Seasonal variations of water masses and sea level in the southwestern part of the Okhotsk Sea. Journal of Oceanography, 56, 643-654.

Kalnay, E., Kanamitsu, M., Kistler, R., Collins, W., Deaven, D., Gandin, L., Iredell, M., Saha, S., White, G., Woollen, J., Zhu, Y.,Leetmaa, A., Reynolds, B., Chelliah, M., Ebisuzaki, W., Higgins, W., Janowiak, J., Mo, K.C., Ropelewski, C., Wang, J., Jenne, R., Joseph, D., 1996. The NCEP/NCAR 40-year reanalysis project. Bulletin of the American Meteorological Society, 77, 437-471.

Kanamitsu, M., 1989. Description of the NMC global data assimilation and forecast system. Weather and Forecasting, 4, 335-342.

Kaplan, D., Glass, L., 1995. *Understanding nonlinear dynamics*. Springer-Verlag, pp. 420.

Katsumata, K., Yasuda, I., 2010. Estimates of non-tidal exchange transport between the Sea of Okhotsk and the North Pacific. Journal of Oceanography, 66, 489-504.

731 Konishi, T., Kamie, E., Segawa, T., 1986. Characteristics of tides along the coast of
732 Japan. Kaiyo Kagaku, 18, 437-441 (in Japanese).
733 Large, W.G., Pond, S., 1981. Open ocean momentum flux measurements in moderate
734 to strong winds. Journal of Physical Oceanography, 11, 324-336.
735 Leppäranta, M., 2005. The drift of sea ice. Springer, Berlin.
736 Leonov, A.K., 1960. *The Sea of Okhotsk*, National Technical Information Service,
737 Springfield, VA, U. S. A.
738 Locarnini, R.A., Mishonov, A.V., Antonov, J.I., Boyer, T.P., Garcia, H.E., 2006. World
739 Ocean Atlas 2005, vol. 1: Temperature, NOAA Atlas NESDIS 61, 182 pp.,
740 NOAA, Silver Spring, Md.
741 Lockridge, P.A., 1995. NGDC monitors frequency of recent destructive tsunami
742 events. Earth System Monitor, 5, 1-12.
743 Masumoto, Y., Sasaki, H., Kagimoto, T., Komori, N., Ishida, A., Sasai, Y., Miyama, T.,
744 Motoi, T., Mitsudera, H., Takahashi, K., Sakuma, H., Yamagata, T., 2004. A
745 fifty-year eddy-resolving simulation for the World Ocean-Preliminary outcomes
746 of OFES (OGCM for the Earth Simulator)-. Journal of the Earth Simulator, 1,
747 35-56.
748 Matsuyama, M., Wadaka, M., Abe, T., Aota, M., Koike, Y., 2006. Current structure
749 and volume transport of the Soya Warm Current in summer. Journal of
750 Oceanography, 62, 197-205.
751 Mizuta, G., Fukamachi, Y., Ohshima, K.I., Wakatsuchi. M., 2003. Structure and
752 seasonal variability of the East Sakhalin Current. Journal of Physical
753 Oceanography, 33, 2430-2445.
754 Mizuta, G., Ohshima, K.I., Fukamachi, Y., Itoh, M., Wakatsuchi, M., 2004. Winter

755 mixed layer and its yearly variability under sea ice in the southwestern part of the
756 Sea of Okhotsk. Continental Shelf Research, 24, 643-657.
757 Mizuta, G., Ohshima, K.I., Fukamachi, Y., Wakatsuchi, M., 2005. The variability of
758 the East Sakhalin Current induced by winds over the continental shelf and slope.
759 Journal of Marine Research, 63, 1017-1039.
760 Morimoto, A., 2009. Evaluation of tidal error in altimetry data in the Asian marginal
761 seas. Journal of Oceanography, 65, 477-485.
762 Nakanowatari, T., Ohshima, K.I., Nagai, S., 2010. What determines the maximum sea
763 ice extent in the Sea of Okhotsk? Importance of ocean thermal condition from
764 the Pacific. Journal of Geophysical Research, 115, C12031,
765 doi:10.1029/2009JC006070.
766 Nishioka, J., Ono, T., Saito, H., Nakatsuka, T., Takeda, S., Yoshimura, T., Suzuki, K.,
767 Kuma, K., Nakabayashi, S., Tsumune, D., Mitsudera, H., Johnson, W.K., Tsuda,
768 A., 2007. Iron supply to the western subarctic Pacific: Importance of iron export
769 from the Sea of Okhotsk. Journal of Geophysical Research, 112, C10012,
770 doi:10.1029/2006JC004055.
771 Ohshima, K.I., 1994. The flow system in the Japan Sea caused by a sea-level
772 difference through shallow straits. Journal of Geophysical Research, 99, C5,
773 9925-9940.
774 Ohshima, K.I., Wakatsuchi, M., Fukamachi, Y., Mizuta, G., 2002. Near-surface
775 circulation and tidal currents of the Okhotsk Sea observed with satellite-tracked
776 drifters. Journal of Geophysical Research, 107, 3195,
777 doi:10.1029/2001JC001005.
778 Ohshima, K.I., Simizu, D., Itoh, M., Mizuta, G., Fukamachi, Y., Riser, S.C.,

779 Wakatsuchi, M., 2004. Sverdrup balance and the cyclonic gyre in the Sea of
780 Okhotsk, Journal of Physical Oceanography, 34, 513–525.
781 Ohshima K.I., Riser, S.C., Wakatsuchi, M., 2005. Mixed layer evolution in the Sea of
782 Okhotsk observed with profiling floats and its relation to sea ice formation.
783 Geophysical Research Letter, 32, L06607, doi:10.1029/2004GL021823.
784 Ohshima, K.I., Nihashi, S., Hashiya, E., Watanabe T., 2006. Interannual variability of
785 sea ice area in the Sea of Okhotsk: importance surface heat flux in fall. Journal of
786 Meteorological Society of Japan, 84, 907-919.
787 Ohshima, K. I., Simizu, D., 2008. Particle tracking experiments on a model of the
788 Okhotsk Sea: Toward oil spill simulation, Journal of Oceanography, 64, 103-114.
789 Ohshima, K.I., Nakanowatari, T., Riser, S.C., Wakatsuchi M., 2010. Seasonal
790 variation in the in- and outflow of the Okhotsk Sea with the North Pacific, Deep
791 Sea Research Part II, 57, 1247-1256.
792 Qiu, B., 2002. Large-scale variability in the midlatitude subtropical and subpolar
793 North Pacific Ocean: Observations and causes. Journal of Physical
794 Oceanography, 32, 353-375.
795 Sadaeva, O., Shevchenko, G., 2001. Investigation of seasonal fluctuations of sea level
796 and atmospheric pressure in the area of Kuril ridge. Proceedings of the 16th
797 international symposium on Okhotsk Sea and Sea Ice, Okhotsk Sea and cold
798 Ocean Research Association, Japan, 339-342.
799 Sakamoto, K., Tsujino H., Nishikawa S., Nakano H., Motoi T., 2010. Dynamics of the
800 Coastal Oyashio and Its Seasonal Variation in a High-Resolution Western North
801 Pacific Ocean Model. Journal of Physical Oceanography, 40, 1283-1301.
802 Sasaki Y.N., Katagiri, Y., Minobe, S., Rigor, I.G., 2007. Autumn atmospheric

803 preconditioning for interannual variability of wintertime sea-ice in the Okhotsk
804 Sea. Journal of Oceanography, 63, 255-265.
805 Shcherbina, A.Y., Talley, L.D., Rudnick, D.L., 2004. Dense water formation on the
806 northwestern shelf of the Okhotsk Sea: 2. Quantifying the transports. Journal of
807 Geophysical Research, 109, C09S09, doi:10.1029/2003JC002197.
808 Shevchenko, G., Romanov, A., 2005. Seasonal variations of surface circulation in the
809 Okhotsk Sea from Topex/Poseidon satellite altimetry data. Proceedings of the
810 20th international symposium on Okhotsk Sea and Sea Ice, Okhotsk Sea and cold
811 Ocean Research Association, Japan, 295-302.
812 Shevhenko, G. V., Chastikov, V. N., 2008. Seasonal variations of oceanic conditions
813 near the southeastern coast of Sakhalin Island. Russian Meteorology and
814 Hydrology, 33, 514-524 (in English).
815 Schlax, M.G. Chelton, D.B., 1994. Aliased tidal errors in TOPEX/POSEIDON sea
816 surface height data. Journal of Geophysical Research, 99, C8, 24761-24775.
817 Shimada, Y., Kubokawa, A., Ohshima, K.I., 2005. Influence of current width variation
818 on the annual mean transport of the East Sakhalin Current: A simple model.
819 Journal of Oceanography, 61, 913-920.
820 Simizu, D., Ohshima, K.I., 2002. Barotropic response of the Sea of Okhotsk to wind
821 forcing. Journal of Oceanography, 58, 851-860.
822 Simizu, D., Ohshima, K.I., 2006. A model simulation on the circulation in the Sea of
823 Okhotsk and the East Sakhalin Current. Journal of Geophysical Research, 111,
824 C05016, doi:10.1029/2005JC002980.
825 Stammer, D., 1997. Steric and wind-induced changes in TOPEX/POSEIDON
826 large-scale sea surface topography observations. Journal of Geophysical

827 Research, 102, C9, 20,987-21,009.
828 Talley, L.D., Nagata, Y., 1995. The Okhotsk Sea and Oyashio Region. PICES
829 Scientific Report, PICES, Sydney, B. C., Canada, 2, 227 pp.
830 Tatebe, H, Yasuda, I., 2005. Numerical experiments on the seasonal variations of the
831 Oyashio near the east coast of Japan. Journal of Physical Oceanography, 35,
832 2309-2326.
833 Trenberth, K.E., Hurrell, J.W., 1994. Decadal atmosphere-ocean variations in the
834 Pacific. Climate Dynamics, 9, 303-319.
835 Tsujino, H., Nakano, H., Motoi T., 2008. Mechanism of currents through the straits of
836 the Japan Sea: Mean state and seasonal variation. Journal of Oceanography, 64,
837 141-161.
838 Uchimoto, K., Mitsudera, H., Ebuchi, N., Mizuta, G., 2008. Seasonal variations of the
839 sea level in the eastern part of the Kuril Basin. Umi to Sora, 84, 93-99 (in
840 Japanese with English abstract and figure captions).
841 Uppala, S.M., Kallberg, P.W., Simmons, A.J., Andrae, U., Da Costa Bechtold, V.,
842 Fiorino, M., Gibson, J.K., Haseler, J., Hernandez, A., Kelly, G.A., Li, X., Onogi,
843 K., Saarinen, S., Sokka, N., Allan, R.P., Andersson, E., Arpe, K., Balmaseda,
844 M.A., Beljaars, A.C.M., van de Berg, L., Bidlot, J., Bormann, N., Caires, S.,
845 Chevallier, F., Dethof, A., Dragosavac, M., Fisher, M., Fuentes, M., Hagemann,
846 S., Ho´ lm, E., Hoskins, B.J., Isaksen, L., Janssen, P.A.E.M., Jenne, R., McNally,
847 A.P., Mahfouf, J.-F., Morcrette, J.-J., Rayner, N.A., Saunders, R.W., Simon, P.,
848 Sterl, A., Trenberth, K.E., Untch, A., Vasiljevic, D., Viterbo, P., Woollen, J., 2005.
849 The ERA-40 re-analysis. Quarterly Journal of the Royal Meteorological Society
850 131, 2961–3012.

851 Vivier, F., Kelly K. A., Thompson L., 1999. Contributions of wind forcing, waves, and
852 surface heating to sea surface height observations in the Pacific Ocean. Journal
853 of Geophysical Research, 104, 20,767-20,788.
854 Woodworth, P.L., 1991. The permanent service for mean sea level and the global sea
855 level observing system. Journal of Coastal Research, 7, 699-710.
856

857 **Figure captions**

858

859 **Fig. 1.** Bathymetry map of the Sea of Okhotsk with the positions of the tide gauge
860 stations used in this study. Filled and open circles indicate the tide gauge stations at
861 which the available data length before 1994 is longer and shorter than 25 years,
862 respectively. The station names from A to O are listed in Table 1. The bathymetry data
863 are derived from the ETOPO5. The contour levels are 100-, 500-, 1000-, and 2000-m
864 depths.

865

866 **Fig. 2.** Time series of monthly sea level (black line) averaged over the tide gauge
867 stations along Sakhalin Island (E, G, H, I, J; see Fig. 1 for locations of the tide gauges)
868 and ATW transport (gray line) for route 1 (see Fig. 5c for the route) from 1965 to
869 1975. The sea level and ATW transport are shown by the anomalies from the averages
870 for the whole period.

871

872 **Fig. 3.** (a) Monthly mean climatologies of the sea level from the tide gauge data (see
873 Fig. 1 for the locations of the tide gauges). (b) Same as (a), but the thermosteric
874 components related to surface heat flux and the inverse barometer effect caused by
875 atmospheric pressure are removed. Black, red, and blue lines indicate the tide gauge
876 data for the northern part of the Sea of Okhotsk including the Kamchatka Peninsula,
877 Sakhalin Island, and the coastal region of Hokkaido Island, respectively.

878

879 **Fig. 4.** Climatological sea level difference (cm) between December and May for (a)
880 the tide gauge data (see Fig. 1 for the locations of the tide gauges) and (b) the satellite
881 altimeter data. In (b), regions in which the sea ice concentration is larger than 10% are

882 masked out by white color.

883

884 **Fig. 5.** (a) Wind stress (vectors; N/m^2) and sea level pressure (contours; hPa) from
885 ERA-40 data for the period 1958–2001 in winter (December to February). The
886 contour interval is 5 hPa. The scale for the vectors is indicated at the bottom. (b) The
887 Sverdrup transport streamfunction in winter. The Sverdrup transport in the Sea of
888 Okhotsk and the North Pacific are calculated independently. The assumed eastern
889 boundary for the Sea of Okhotsk is shown as a bold line. The contour intervals are 2
890 Sv and 10 Sv in the Sea of Okhotsk and the North Pacific, respectively. (c) The
891 integral routes for the ATW transport. In (c), the integral routes 1, 2, and 3 are defined
892 as the line from the corresponding starting points to the end point each marked with
893 an open circle. The label of S, P, K indicates the Sakhalin, Petropavlovsk–Kamchatsky,
894 and Kushiro stations, respectively.

895

896 **Fig. 6.** (a) The monthly mean climatologies of the tide gauge sea level averaged along
897 Sakhalin Island (D–J). (b) The monthly mean climatologies of the ATW transport
898 integrated over routes 1 (circle), 2 (triangle), and 3 (cross). The scale of the ATW
899 transport for route 1 and 2 (3) is indicated on the left (right) axis. (c) The monthly
900 mean climatologies of the Sverdrup transport over the Sea of Okhotsk (circle) and
901 North Pacific (triangle). The scale for the Sverdrup transport in the Sea of Okhotsk
902 (North Pacific) is indicated on the left (right) axis.

903

904 **Fig. 7.** Longitudinal dependence of the differences in the sea level, ATW transport,
905 and Sverdrup transport between December and May. (a) Tide gauge data along the

906 Sakhalin coast (station labels are indicated at the top). (b) ATW transport integrated
907 from the starting point of route 1 to the corresponding latitude at the Sakhalin coast.
908 (c) Sverdrup transport integrated over the Sea of Okhotsk (circle) and the North
909 Pacific (triangle). In (c), the scale for the Sverdrup transport in the Sea of Okhotsk
910 (North Pacific) is indicated on the left (right) axis.
911
912 **Fig. 8.** Time series of the sea level anomalies (cm) at the tide gauge stations in winter
913 (December to February) (see Fig. 1 for the locations of the tide gauges) and the
914 temporal coefficients of the first EOF mode from the 11 tide gauge data in winter.
915 Note that the sea level anomalies for each station are successively offset by 15 cm.
916
917 **Fig. 9.** (a) Regression maps (colors) of the sea level anomalies onto the PC1 of the
918 tide gauge sea levels in winter (December–February). (b) Regression maps (colors) of
919 the December SSHAs onto the normalized SSHAs averaged over the area offshore of
920 Sakhalin Island (48–49°N, 143–144°E; indicated as green square). Contours indicate
921 the areas where the correlation exceeds the 95% confidence level. The regions in
922 which the sea ice concentration is larger than 10% are masked out by white.
923
924 **Fig. 10.** Time series of the wintertime (December to February) sea level anomalies
925 (solid line) averaged along Sakhalin Island (E, G, H, I, J) (see Fig. 1 for the locations)
926 and the ATW transport anomalies (dashed line) for route 1 (see Fig. 5c for the route
927 location).
928
929 **Fig. 11.** Regression maps of (a) the wind stress, (b) wind stress curl, and (c) sea level

930 pressure onto the PC-1 of the sea levels in winter (December to February). In (a), the
931 standard vector length of 0.03 N/m^2 is shown at the bottom. The contour intervals in
932 (b) and (c) are 0.2 N/m^3 and 0.5 hPa, respectively. Light (heavy) shading indicates the
933 region in which the positive (negative) correlation is significant at the 95% confidence
934 level.
935
936 **Fig. 12.** The time series of the PC-1 (solid line) of the wintertime (December to
937 February) sea levels and the sea ice extent anomalies in January (dashed line).
938

939 **Table 1**

940 Locations of the tide gauge stations and the available data period

Station Label	Station Name	Latitude	Longitude	Data Period
A	Petropavlovsk-Kamchatsky[a]	52°59’N	158°39’E	1958–2009
B	Nagaevo	59°33’N	150°43’E	1957–1993
C	Okhotsk	59°22’N	143°12’E	1972–1993
D	Nabil	51°44’N	143°18’E	1960–1964
E	Poronaisk	49°14’N	143°08’E	1950–1993
F	Vostochniy	48°17’N	142°35’E	1948–1957
G	Vzmorie	47°52’N	142°29’E	1950–1988
H	Starodubskoe	47°25’N	142°49’E	1950–1993
I	Korsakov	46°39’N	142°45’E	1948–1992
J	Krilion	45°54’N	142°05’E	1961–1988
K	Wakkanai[a]	45°24’N	141°41’E	1975–2009
L	Monbetsu[a]	44°21’N	143°22’E	1956–2008
M	Abashiri[a]	44°01’N	144°17’E	1965–2009
N	Kurilsk	45°16’N	147°53’E	1951–1993
O	Kushiro[a]	42°58’N	144°22’E	1947–2009

941 [a] Data from the PSMSL.

942

943

Table 2

Correlation coefficients between the sea level along Sakhalin Island and the Sverdrup transport integrated over the Sea of Okhotsk (OK) and North Pacific (NP) and the ATW transport integrated along routes 1, 2, and 3 (ATW-1, -2, and -3), calculated using ERA-40 and NCEP/NCAR reanalysis data in winter (December to February)

	OK	NP	ATW-1	ATW-2	ATW-3
ERA40	**0.64**	**0.37**	**0.66**	**0.53**	**0.62**
NCEP-NCAR	**0.71**	0.34	**0.71**	**0.68**	**0.69**

Bold numbers indicate correlations exceeding the 95% confidence level based on the Monte Carlo simulation, using a phase randomization technique generating 1,000 surrogate time series (Kaplan and Glass, 1995).

954 **Table 3**

955 Correlation coefficients between the sea level along Sakhalin Island and ATW
956 transport for routes 1 and 3 in winter (December to February), spring (March to May),
957 summer (June to August), and autumn (September to November)

	Winter	Spring	Summer	Autumn
ATW-1	**0.66**	0.25	-0.07	0.42
ATW-3	**0.62**	0.03	-0.17	-0.01

958 Bold numbers indicate the correlation exceeding the 95% confidence level.

959

960

961 **Table 4**

962 Correlation coefficients between the tide gauge sea level anomalies at
963 Petropavlovsk–Kamchatsky (PK) and Kushiro and the corresponding ATW transport
964 and Sverdrup transport in the North Pacific in winter (December to February)

	ATW	Sverdrup transport
PK	**0.65**	**0.59 (at 51°N)**
Kushiro	**0.59**	**0.56 (at 42°N)**

965 Bold numbers indicate the correlations exceeding the 95% confidence level.

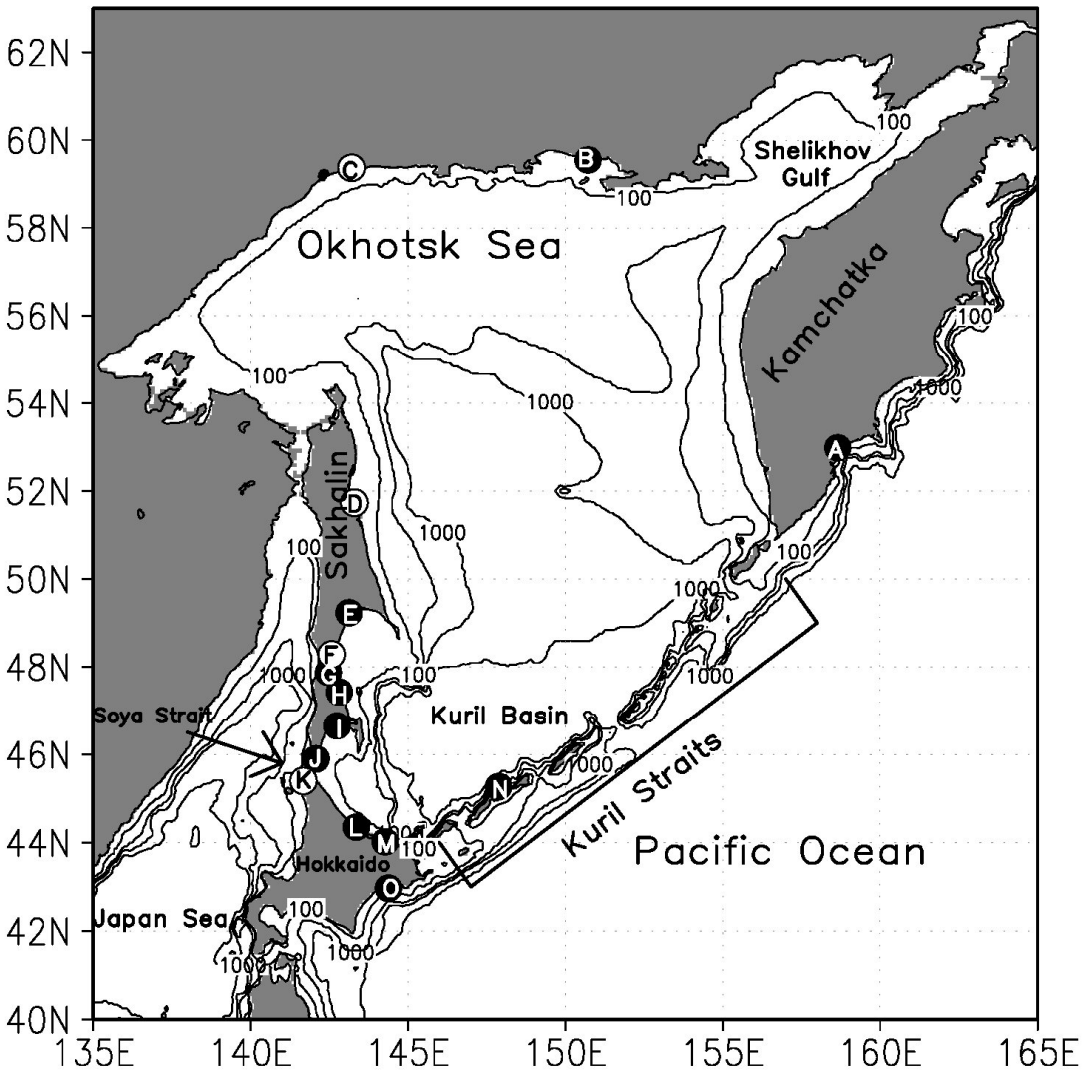

966

967 **Figure 1.**

968

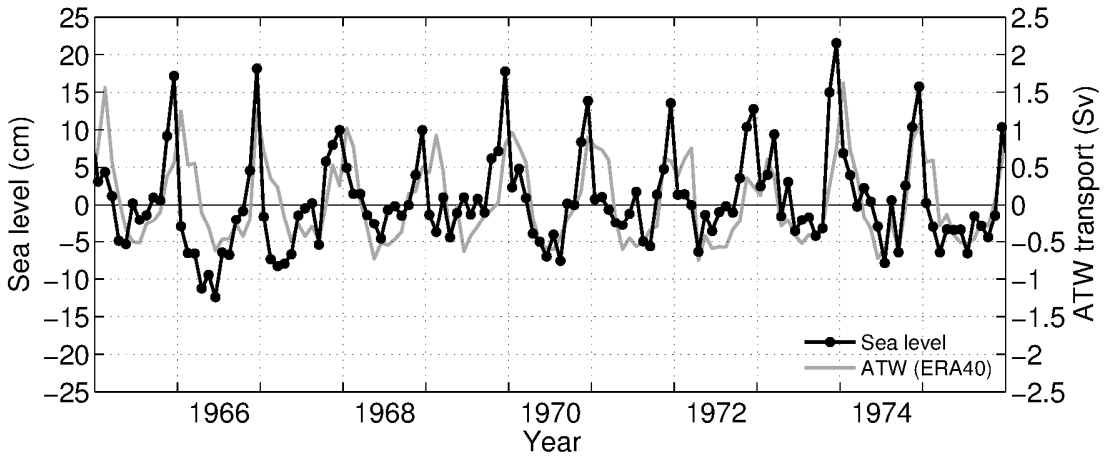

969

970 **Figure 2.**

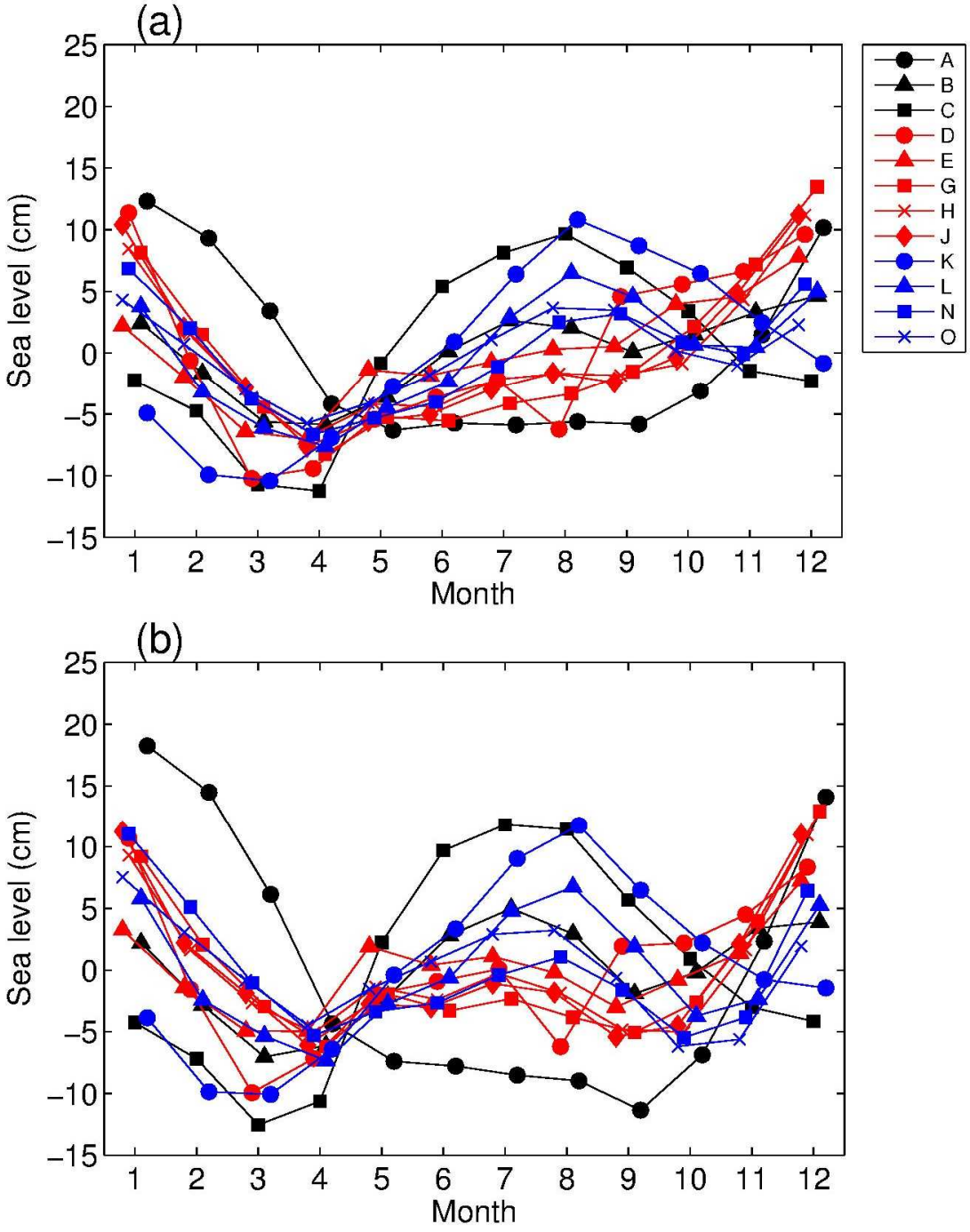

971

972 **Figure 3.**

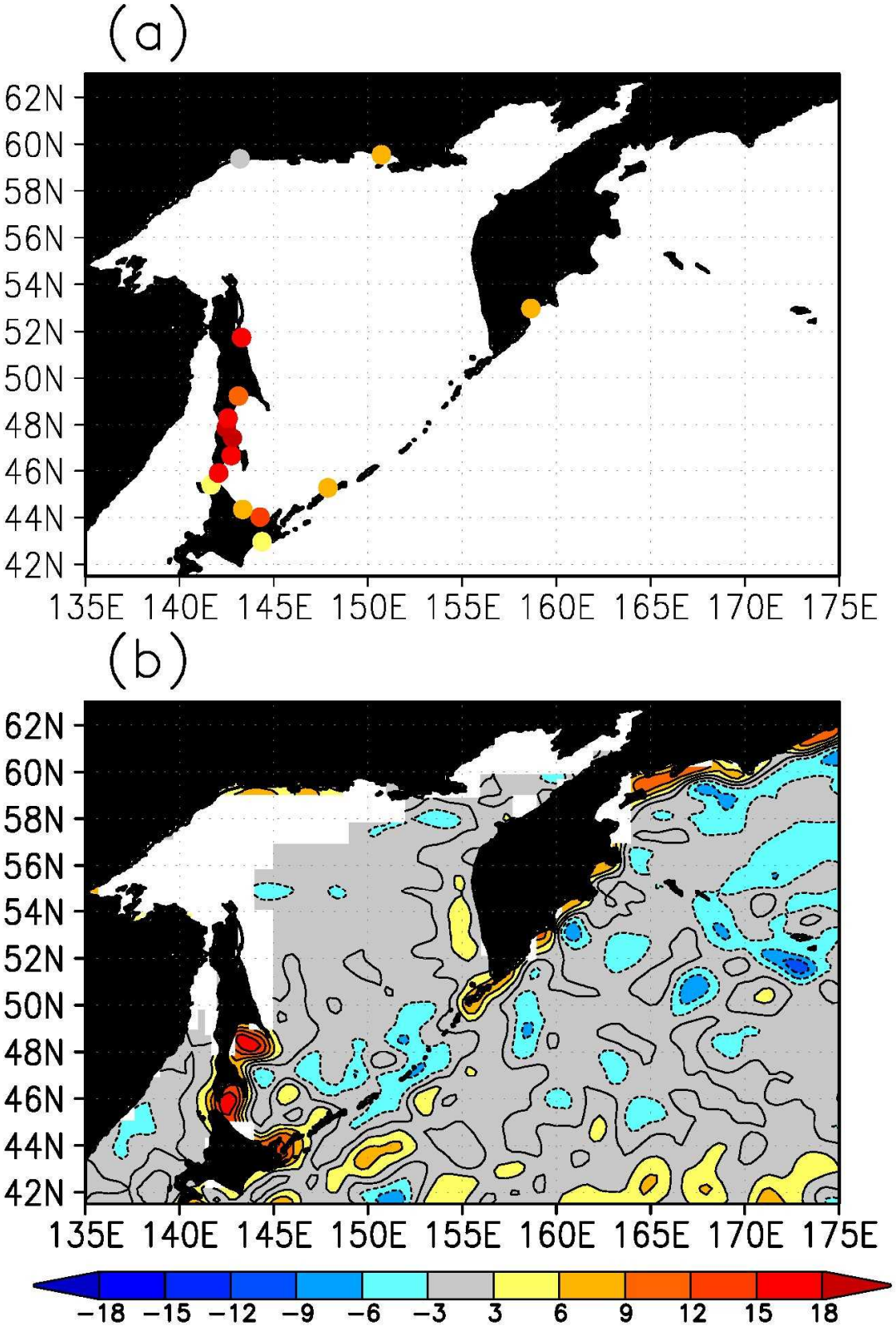

973

974 **Figure 4.**

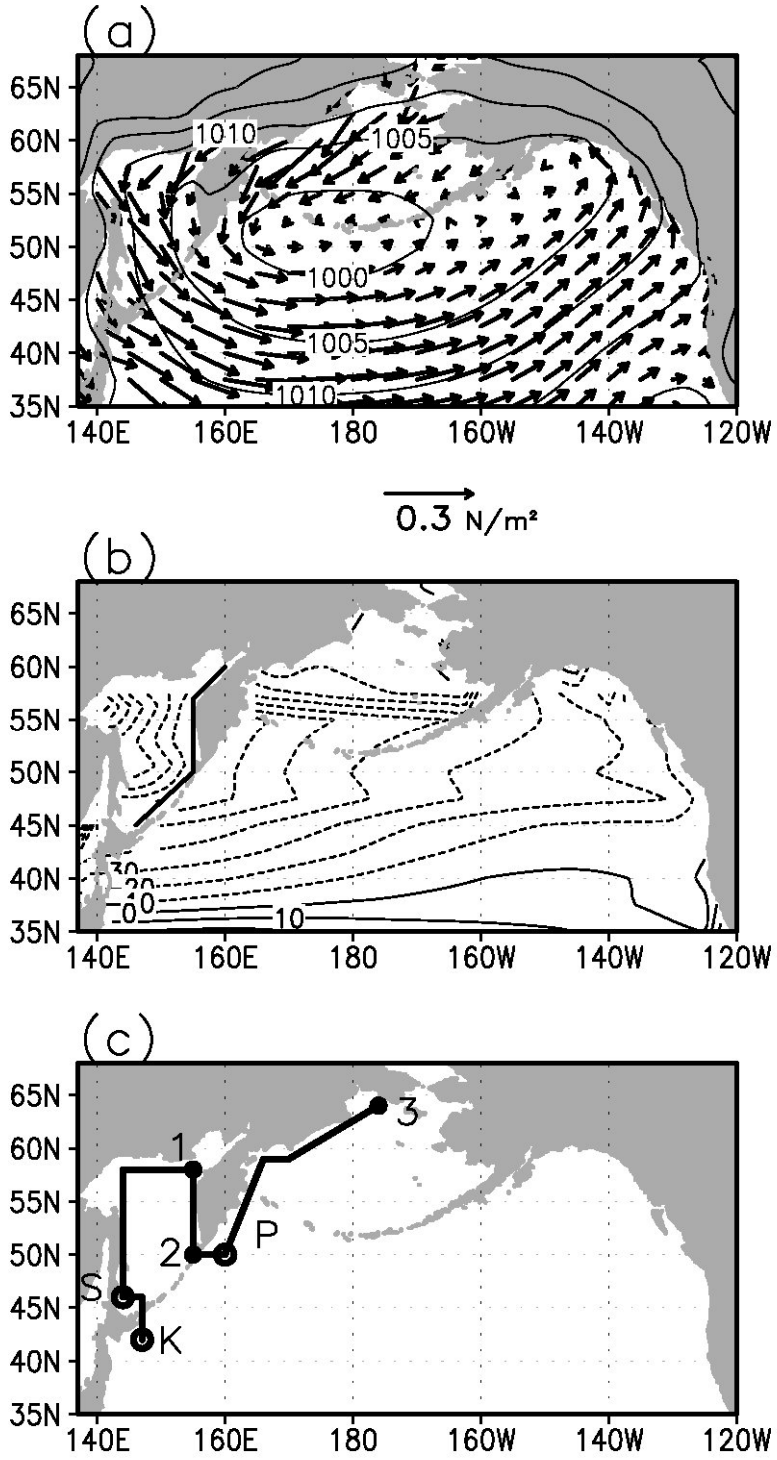

975

976 **Figure 5.**

977

978

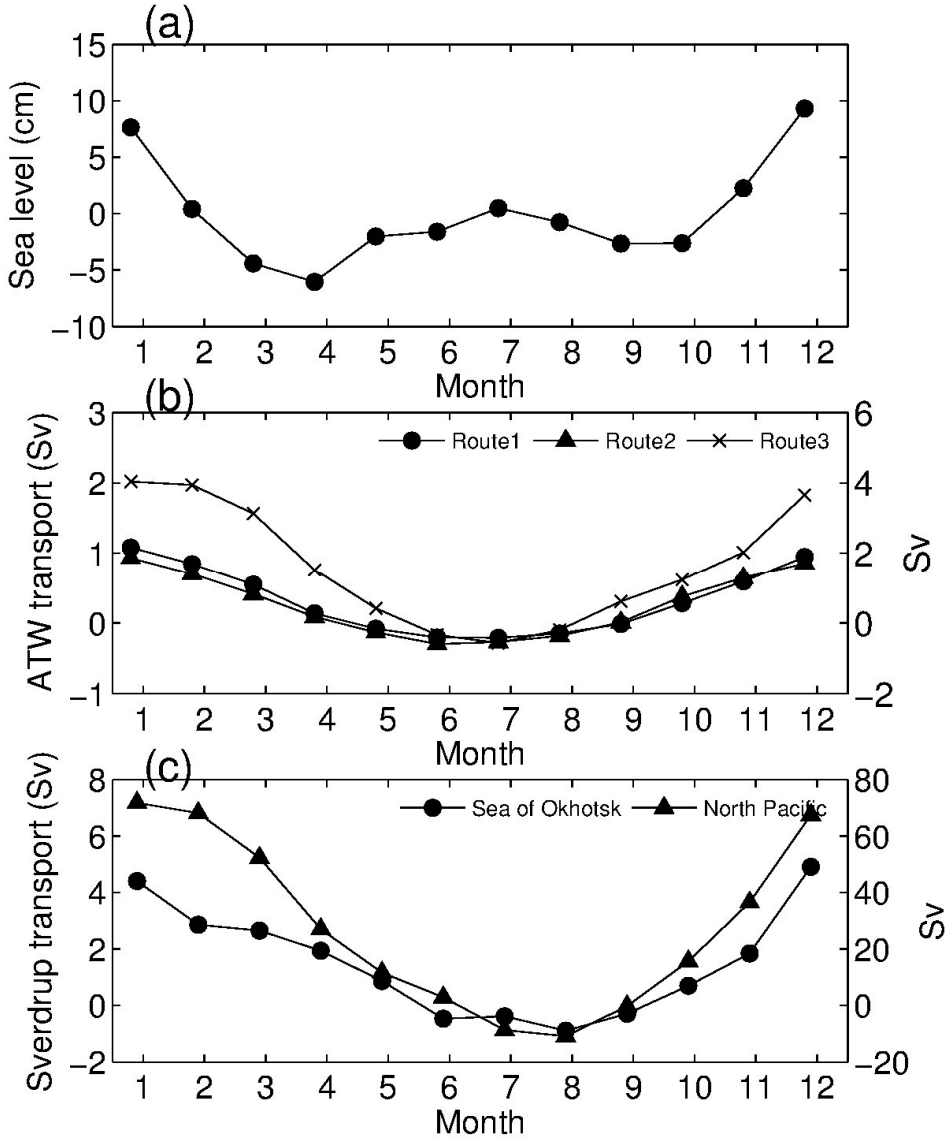

979

980 **Figure 6.**

981

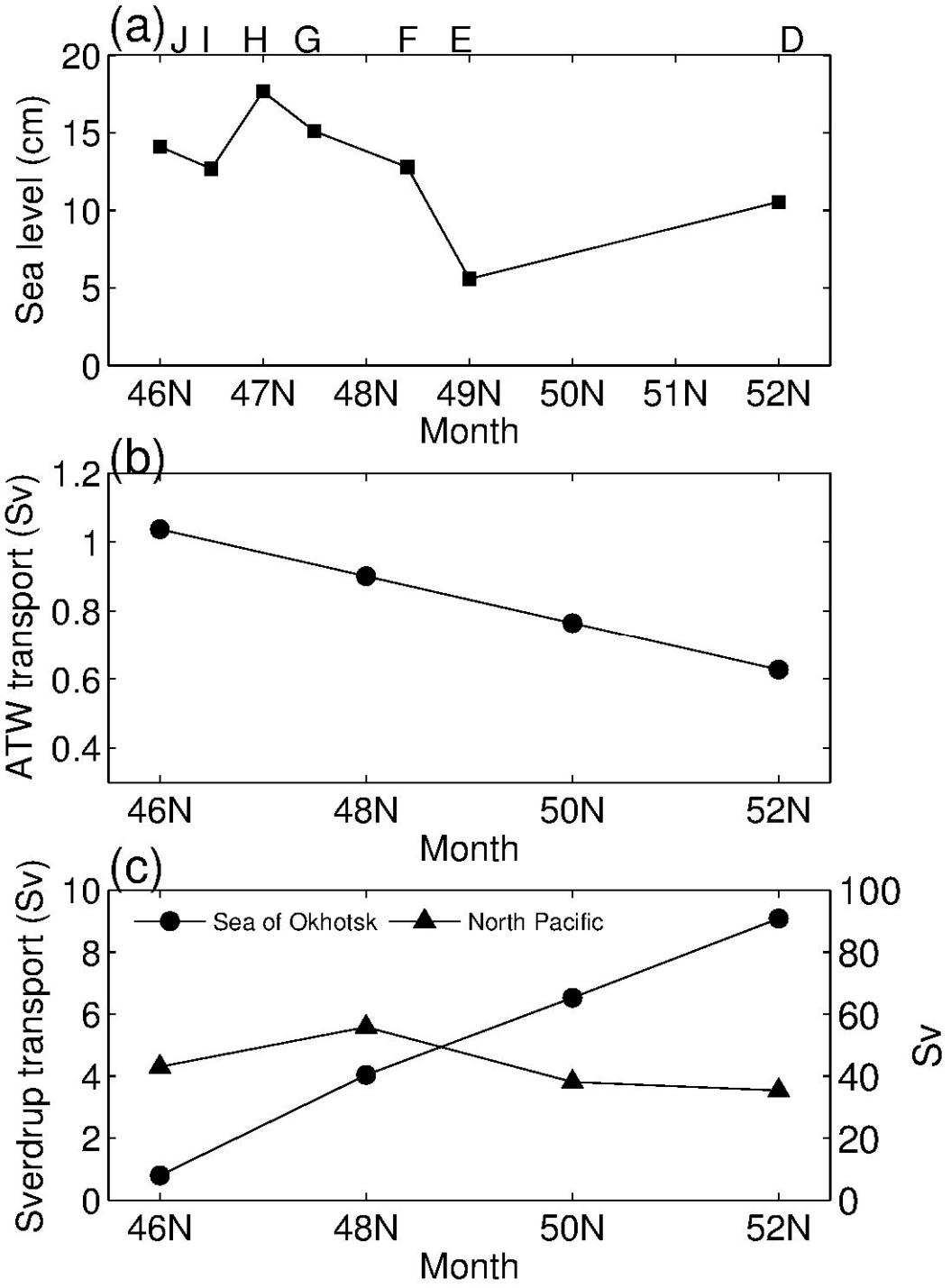

982

983 **Figure 7.**

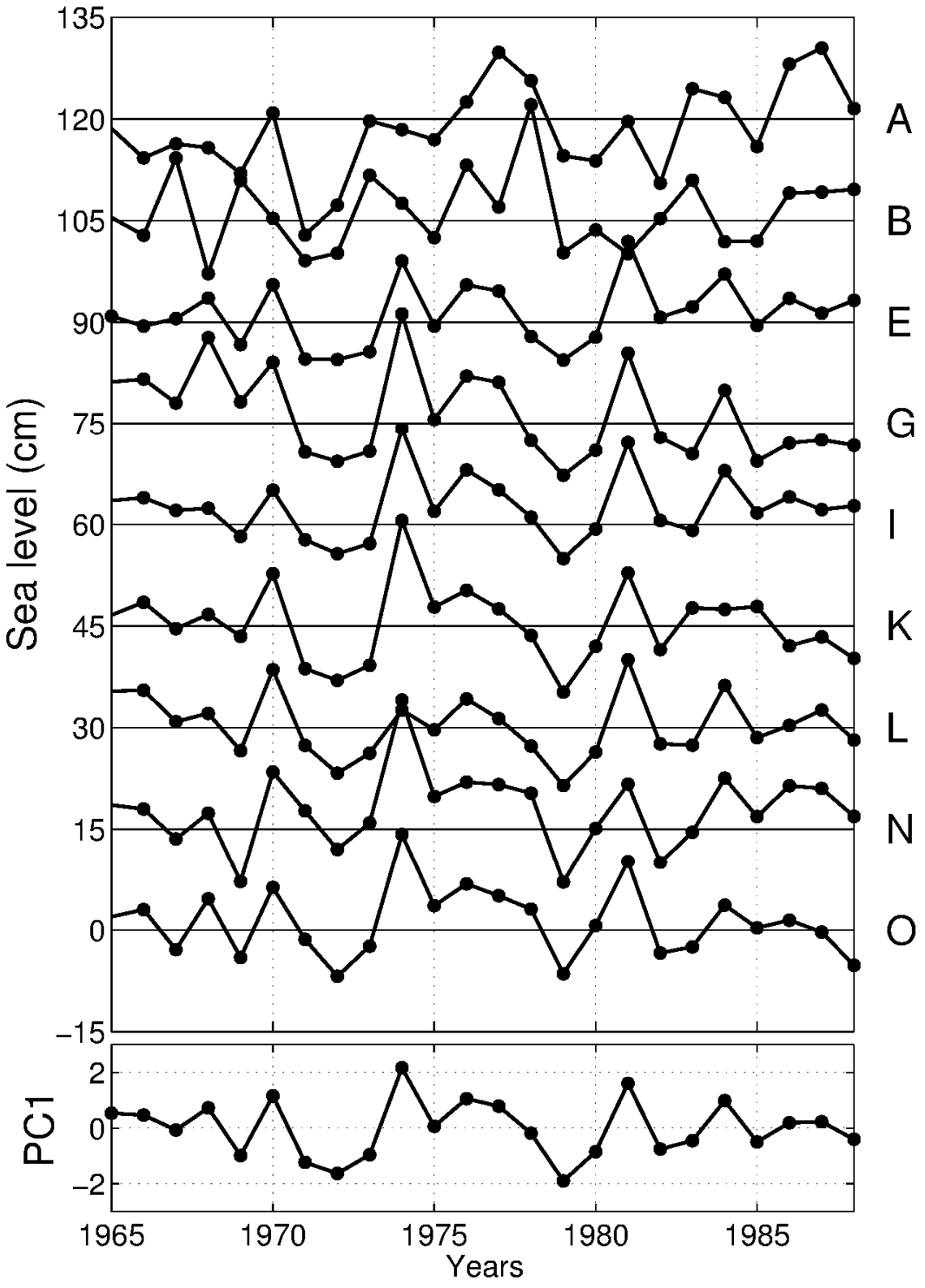

984

985 **Figure 8.**

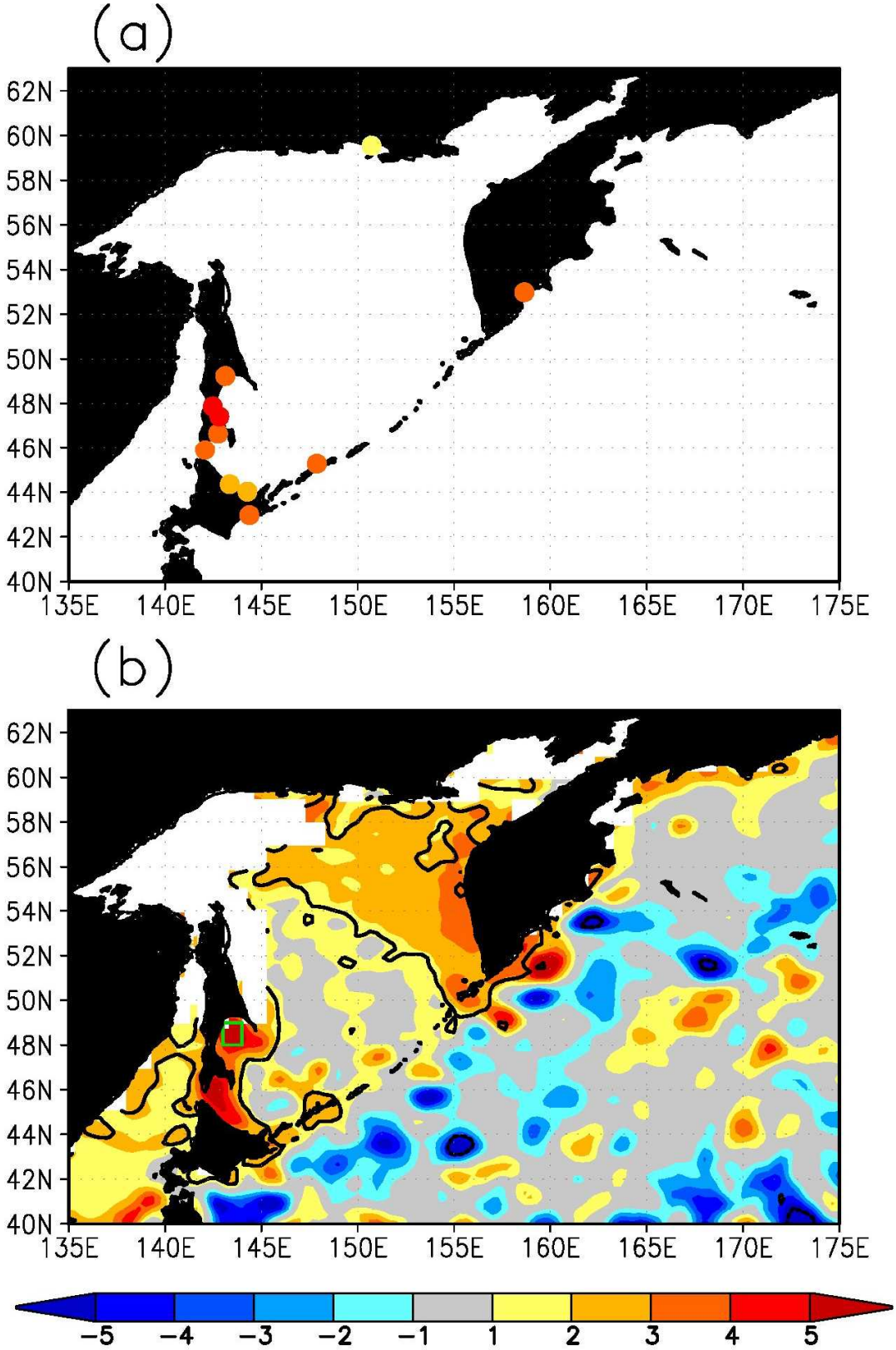
(a)
62N
60N
58N
56N
54N
52N
50N
48N
46N
44N
42N
40N
135E
140E
145E
150E
155E
160E
165E
170E
175E
(b)
62N
60N
58N
56N
54N
52N
50N
48N
46N
44N
42N
40N
135E
140E
145E
150E
155E
160E
165E
170E
175E
−5
−4
−3
−2
−1
1
2
3
4
5

Figure 9.

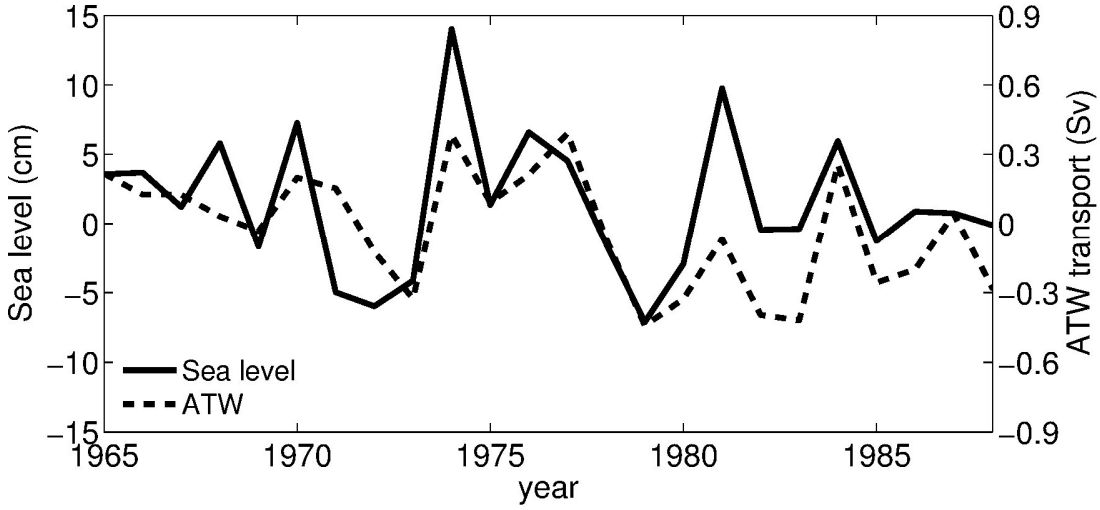
Sea level (cm)
ATW transport (Sv)
year
Sea level
ATW
15
10
5
0
−5
−10
−15
0.9
0.6
0.3
0
−0.3
−0.6
−0.9
1965
1970
1975
1980
1985

Figure 10.

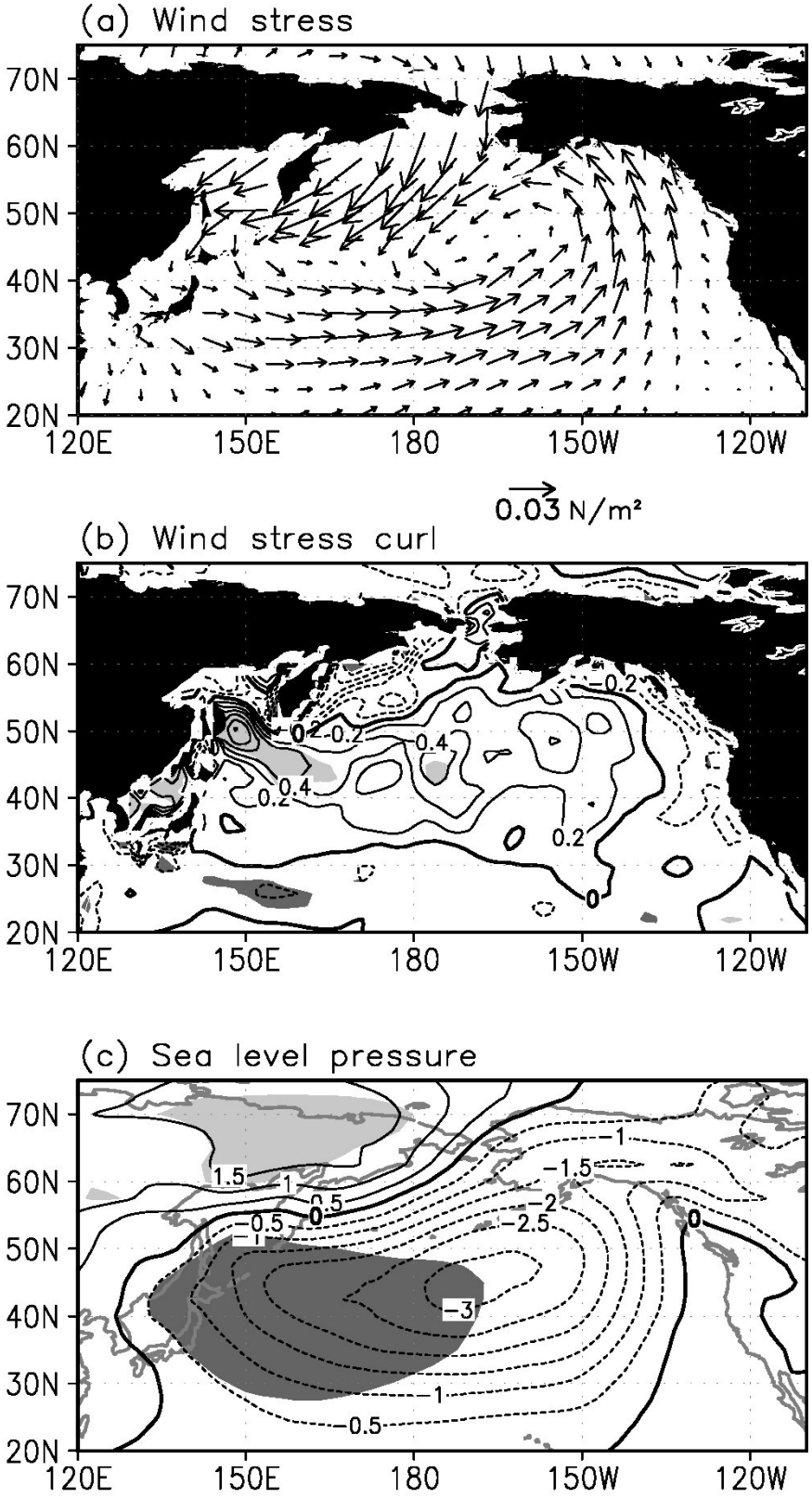

990

991 **Figure 11.**

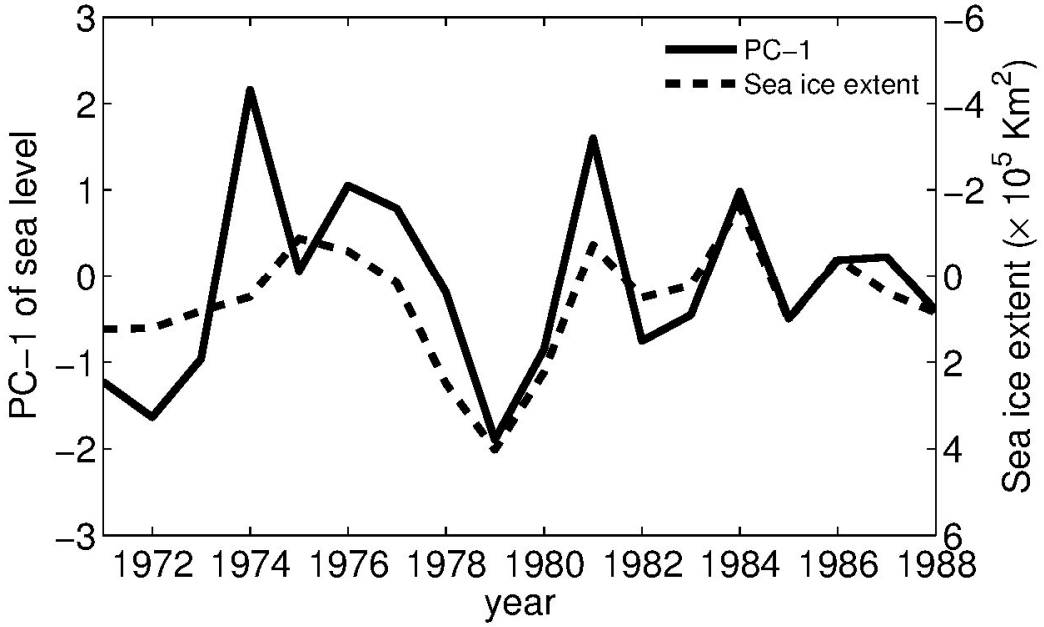

992

993 **Figure 12.**